
PERSONALIZED TREATMENT SELECTION VIA PRODUCT PARTITION MODELS WITH COVARIATES

Matteo Pedone

Department of Statistics, Computer Science and Applications
University of Florence
matteo.pedone@unifi.it

Raffaele Argiento

Department of Economics
University of Bergamo
raffaele.argiento@unibg.it

Francesco C. Stingo

Department of Statistics, Computer Science and Applications
University of Florence
francescoclaudio.stingo@unifi.com

ABSTRACT

Precision medicine is an approach for disease treatment that defines treatment strategies based on the individual characteristics of the patients. Motivated by an open problem in cancer genomics, we develop a novel model that flexibly clusters patients with similar predictive characteristics and similar treatment responses; this approach identifies, via predictive inference, which one among a set of treatments is better suited for a new patient. The proposed method is fully model-based, avoiding uncertainty underestimation attained when treatment assignment is performed by adopting heuristic clustering procedures, and belongs to the class of product partition models with covariates, here extended to include the cohesion induced by the Normalized Generalized Gamma process. The method performs particularly well in scenarios characterized by considerable heterogeneity of the predictive covariates in simulation studies. A cancer genomics case study illustrates the potential benefits in terms of treatment response yielded by the proposed approach. Finally, being model-based, the approach allows estimating clusters' specific response probabilities and then identifying patients more likely to benefit from personalized treatment.

1 Introduction

Cancer comprises a collection of complex diseases characterized by heterogeneous cellular alterations across patients and cancer cells within the same neoplasm (Bedard et al., 2013). Patients with similar clinical diagnoses may show diverse responses to the same treatment due to tumor heterogeneity. A treatment for a particular diagnosis may be effective on average, but its effectiveness may vary across subpopulations. In recent years many attempts have been made to devise personalized treatment strategies that leverage patients' characteristics, including the tumor's genome, to identify the treatment with the highest likelihood of success (Simon, 2010). Within this precision medicine paradigm, there is an increasing interest in discovering individualized treatment rules (ITRs) for patients that show heterogeneous responses to treatment, e.g., when the treatment effect varies across groups of patients. An ITR is a decision rule that assigns the patient to the treatment given patient/disease characteristics (Ma et al., 2015). The optimal ITR is the one that maximizes the population mean outcome. Statistical methodology research in precision medicine is devoted to developing personalized treatment rules to inform decision-making. The distinctive mark of statistical inference under the precision medicine paradigm is to leverage heterogeneity to improve therapeutic strategies (Kosorok and Laber, 2019).

Our interest specifically lies in developing frontline treatment selection rules rather than estimating treatment's causal effects, as commonly done within the ITR framework. Conventional methods for treatment selection rules are based on semi- and non-parametric procedures to identify subgroups of patients more likely to benefit from a treatment leveraging few baseline markers (Bonetti and Gelber, 2000; Song and Pepe, 2004). The subgroup approach can provide

valuable information when performed according to a prespecified analysis plan. Nonetheless, stratified subsets of patients defined by one or few biomarkers are often inadequate to account for patient heterogeneity and ultimately fail to establish effective treatment selection rules (Pocock et al., 2002). Other approaches account for patient heterogeneity by including covariates (Zhang et al., 2012; Zhao et al., 2012). However, for these methods, the correct definition of treatment-by-markers interactions is crucial and relies on sensitive assumptions, which are difficult to specify in the clinical practice and may be limited to generalized linear models (Ma et al., 2016).

To overcome these limitations, Ma et al. (2016, 2018, 2019) have established a hybrid two-step predictive model for personalized treatment selection. In the first step, a clustering algorithm based on a pre-defined genomic signature (predictive markers) is used to obtain a heuristic measure of the patients' molecular similarity. In the second step, given this measure of patients' similarity and a set of prognostic markers, a Bayesian model is used for treatment selection; specifically, for a new, untreated patient, the model predicts the treatment response probabilities for each competing treatment. This framework establishes two significant improvements over existing methods. Firstly, the common assumption of statistical exchangeability among patients is relaxed. Since each tumor is unique, patients are considered partially exchangeable only to the extent to which their tumors are molecularly similar. Moreover, this approach utilizes complementary sources of information for treatment selection, integrating predictive and prognostic characteristics of a patient.

This paper proposes a Bayesian predictive model for personalized treatment selection that builds upon Ma et al. (2019) and overcomes some of its main limitations. As in Ma et al. (2019), we leverage prognostic determinants and predictive biomarkers for treatment selection. We propose a fully Bayesian integrative framework for clustering and prediction that performs all inferential tasks in a single model avoiding multi-step procedures; the proposed approach results in a treatment selection rule that fully accounts for patients' heterogeneity. Note that in Ma et al. (2019), the patients' similarities were estimated in the first step and included as known quantities in the second step; moreover, in the first step, two arbitrary choices had to be made, namely the clustering algorithm and the number of clusters. The proposed method accounts for the uncertainty in all modeling steps, resulting in improved prediction performances. In particular, we use a product partition model with covariates (PPMx, Müller et al., 2011) to cluster observations that are similar in terms of the values of the predictive covariates; specifically, the predictive covariates enter the model through the prior for the random partition. The resulting partitions are only partially exchangeable, and patients with similar covariates are *a priori* more likely to be clustered together. In this paper, we use the *cohesion function* induced by the Normalized Generalized Gamma process (NGGP) as a building block of our PPMx model to mitigate the *rich-get-richer* property of the Bayesian nonparametric (BNP) priors. Namely, the *rich-get-richer* is the tendency for a small number of clusters to become overrepresented as more data points are added to the process, resulting in few large clusters and potentially many singletons. Despite being well studied in the Bayesian nonparametric literature as a prior inducing a Gibbs-type random partition (Lijoi et al., 2007), NGGP still has no common use. To the best of our knowledge, this is one of the first attempts the NGGP is employed as *cohesion function* in a PPMx model (see Argiento et al., 2022).

We devise a method that, given the patients' prognostic and predictive markers, assigns them to the treatment with the highest likelihood of positive response. Prognostic covariates influence disease progression regardless of the treatments given to the patient, whereas predictive covariates change the likelihood of a positive response to a particular treatment. Conceptually, our strategy for selecting the optimal treatment for the new, untreated patient can be broken down into three steps. First, we consider historical patients and cluster them separately for each treatment according to their predictive markers. In this way, patients that underwent the same treatment are divided into homogeneous clusters with respect to predictive biomarkers. Then, we compute the utility provided by each competing treatment to the new untreated patient by assigning the new patient to the subgroup of historical patients with whom he shows the largest similarity in terms of predictive markers. The utility function relies on the model's posterior predictive distribution, which depends on both prognostic and predictive biomarkers. Finally, we select the treatment that ensures the largest predicted benefit.

We apply the proposed method to a brain cancer dataset (Ma et al., 2019), comprising 158 patients equally assigned to either standard or targeted treatment. For each patient, prognostic and predictive biomarkers, both consisting of pre-selected genomics markers, are available in addition to their categorical response to treatment. To facilitate optimal treatment selection, we assign numerical utilities to each treatment response level. This leads to a median utility score, which serves as a one-dimensional criterion for treatment selection. Our model shows good predictive performances and provides a sound framework for the identification and interpretation of clusters of patients.

2 Bayesian Integrative Model

We consider n historical patients treated with T alternative treatments, whose predictive and prognostic biomarkers are measured along with a discrete set of response levels of the clinical outcome. Let $a = 1, \dots, T$ index treatments

and $n = \sum_{a=1}^T n^a$ be the total number of treated patients, of which n^a assigned to therapy a . Note that, in our notation the superscript a is solely a treatment index. The treatment response y_i^a of patient i is a categorical variable with K levels that encodes the residual disease extent after a clinically relevant post-therapy follow-up period. In particular, y_i^a follows a multinomial distribution $y_i^a | \pi_i^a \stackrel{\text{ind}}{\sim} \text{Multinomial}(1, \pi_i^a)$, for $i = 1, \dots, n^a$, with associated probability vector $\pi_i^a = (\pi_{i1}^a, \dots, \pi_{iK}^a)^\top$; π_{ik}^a is the probability of observing outcome k for the i -th patient under treatment a , for $k = 1, \dots, K$. These probabilities will depend on z_i^a and \mathbf{x}_i^a , the P - and Q -dimensional vector of prognostic and predictive features measured on the i -th patient that received treatment a , respectively. We assume that patients with similar predictive biomarkers and the same prognostic covariates will respond similarly to a given treatment. To quantify the effectiveness of each competing treatment for patients with similar values of the predictive biomarkers, we adopt a covariate-dependent random partition model (RPM). For each treatment $a = 1, \dots, T$, patients receiving treatment a are partitioned into clusters based on their predictive biomarkers \mathbf{x}^a . Namely, we make the random partitions depend on predictive biomarkers. Section 4 will describe the covariate-dependent RPM we use to achieve this goal. In this section, we assume that $\mathcal{P}_{n^a}^a = \{S_1^a, \dots, S_{C_{n^a}^a}^a\}$ is a given treatment-specific partition of the indices $\{1, \dots, n^a\}$, where $C_{n^a}^a$ is the number of clusters among patients treated with therapy a and $n_j^a = |S_j^a|$ is the cardinality of cluster j , for $j = 1, \dots, C_{n^a}^a$. Since we will later treat the partition of the units as a random quantity, the partition itself and the number of clusters depend on the number of observations, n^a . Following a common convention, we identify cluster-specific quantities using the superscript “ \star ”. For example, when considering cluster S_j^a , the response vector is $\mathbf{y}_j^{a\star} = \{y_i^a : i \in S_j^a\}$, while $\mathbf{x}_j^{a\star} = \{\mathbf{x}_i^a : i \in S_j^a\}$ is the partitioned covariate matrix. We define the following hierarchical model for the response variables:

$$\begin{aligned} y_i^a | \pi_i^a &\stackrel{\text{ind}}{\sim} \text{Multinomial}(1, \pi_i^a) \\ \pi_1^a, \dots, \pi_{n^a}^a | \boldsymbol{\eta}_1^{a\star}, \dots, \boldsymbol{\eta}_{C_{n^a}^a}^{a\star}, \mathcal{P}_{n^a}^a, \boldsymbol{\beta} &\sim \prod_{j=1}^{C_{n^a}^a} \prod_{i \in S_j^a} \text{Dirichlet}(\gamma_i^a(\boldsymbol{\eta}_j^{a\star}, \boldsymbol{\beta})), \end{aligned} \quad (2.1)$$

where $\gamma_i^a(\boldsymbol{\eta}_j^{a\star}, \boldsymbol{\beta}) = (\gamma_{i1}^a(\boldsymbol{\eta}_j^{a\star}, \boldsymbol{\beta}_1), \dots, \gamma_{iK}^a(\boldsymbol{\eta}_j^{a\star}, \boldsymbol{\beta}_K))^\top$ is a vector of log-linear functions of the prognostic markers and cluster-specific parameters defined as follows:

$$\log(\gamma_{ik}^a(\boldsymbol{\eta}_j^{a\star}, \boldsymbol{\beta}_k)) = \eta_{jk}^{a\star} + \beta_{1k} z_{i1}^a + \dots + \beta_{Pk} z_{iP}^a. \quad (2.2)$$

Model (2.1) is robust with respect to overdispersion (Corsini and Viroli, 2022), which is usually observed in multivariate categorical data (Chen and Li, 2013). Predictive biomarkers, \mathbf{x}^a , enter equation (2.2) through the parameter vectors $\boldsymbol{\eta}_1^a, \dots, \boldsymbol{\eta}_{C_{n^a}^a}^a$ and the partition $\mathcal{P}_{n^a}^a$ that depends on the predictive covariates \mathbf{x}^a , as we will elaborate in Section 3. The K -dimensional vectors $\boldsymbol{\eta}_1^{a\star}, \dots, \boldsymbol{\eta}_{C_{n^a}^a}^{a\star}$ are cluster-specific parameters; high values of $\eta_{jk}^{a\star}$ correspond to an high probability of observing response k for an individual treated with treatment a in cluster j . We enforce $\boldsymbol{\eta}_j^{a\star}$ to be treatment-specific, and, as a consequence, the partitions $\{\mathcal{P}_{n^a}^a\}_{a=1, \dots, T}$ are independent across treatments. This construction provides a comparison among competing treatments. In fact, it allows patients with close genetic profiles that received different treatments to have distinct response probabilities. Finally, $\boldsymbol{\beta} = (\boldsymbol{\beta}_1, \dots, \boldsymbol{\beta}_K)$ is a $P \times K$ matrix of regression parameters shared across treatments. Prognostic biomarkers enter equation (2.2) as linear terms. Since prognostic determinants impact the likelihood of achieving a given therapeutic response regardless of the treatment, the associated coefficients are defined across therapies. Thus, prognostic covariates set a baseline response probability measure. Since patients should not be regarded as statistically exchangeable with respect to predictive biomarkers (Ma et al., 2016), we leverage predictive biomarkers to drive the clustering process within each treatment. The resulting cluster-specific parameters $\boldsymbol{\eta}_j^{a\star}$ assess the benefit offered by a specific treatment on groups of similar patients. Note that the linear predictor is a function of the prognostic biomarkers only: the predictive covariates enter non-linearly equation (2.2) only through the cluster- and treatment-specific parameters $\boldsymbol{\eta}_j^{a\star}$. This construction results in a random intercept that estimates the adjustment provided by predictive biomarkers to the baseline prognostic response probability on account of groups of patients with close predictive determinants. Note that, while the Multinomial logit model (Agresti, 2019) could have provided similar predictive performance, its interpretation would have been less straightforward since the parameters represent log odds ratios with respect to a specific baseline response level.

3 Prior distributions

We assume independent shrinkage priors for the parameters $\boldsymbol{\beta}_k$. In particular, we adopt horseshoe priors (Carvalho et al., 2010), which belong to the class of global-local scale mixtures of normals. More in details, for $p = 1, \dots, P$ and $k = 1, \dots, K$

$$\beta_{pk} \stackrel{\text{iid}}{\sim} N(0, \lambda_{pk}^2 \tau_k^2), \quad \lambda_{pk}, \tau_k \stackrel{\text{iid}}{\sim} HC(0, 1),$$

where HC denotes a half-Cauchy distribution, $\{\lambda_{pk}\}$ are local shrinkage parameters, and $\{\tau_k\}$ are global shrinkage parameters. All coefficients will be nonzero, but only those supported by the data will have large values due to the heavy tails of the prior. The joint distribution of the clustering and the cluster-specific parameters $(\mathcal{P}_n^a, \boldsymbol{\eta}_j^{a*})$, is assumed to be independent across treatments. Therefore we will omit the superscript a throughout Sections 3 and 4. In particular, we assume a product partition model with covariates (PPMx, Müller et al., 2011), that induces independence across clusters and conditional independence within clusters. We detail our proposal for the PPMx on \mathcal{P}_n in Section 4. Here, given \mathcal{P}_n , we details the prior for $\boldsymbol{\eta}_j^*, j = 1, \dots, C_n$. We assume conditional independence between clusters, that is $\boldsymbol{\eta}_j^* \sim G_0$, for $j = 1, \dots, C_n$, where G_0 is a prior for cluster-specific parameters. Then, the joint law of $(\mathcal{P}_n, \boldsymbol{\eta}_j^*)$ is assigned hierarchically as:

$$\boldsymbol{\eta}_j^* \stackrel{\text{iid}}{\sim} G_0, \text{ for } j = 1, \dots, C_n, \quad \mathcal{P}_n \mid \mathbf{x} \sim PPMx(\mathbf{x}).$$

Specifically, we take G_0 to be a K -dimensional multivariate normal distribution and assume that $\boldsymbol{\eta}_j^* \mid \boldsymbol{\theta}, \boldsymbol{\Lambda} \stackrel{\text{iid}}{\sim} N_K(\boldsymbol{\theta}, \boldsymbol{\Lambda}^{-1})$. To achieve more flexibility, we add an extra layer of hierarchy by assuming $\boldsymbol{\theta} \mid \boldsymbol{\mu}_0, \boldsymbol{\Lambda}, \nu_0 \sim N_K(\boldsymbol{\mu}_0, (\nu_0 \boldsymbol{\Lambda})^{-1})$ and $\boldsymbol{\Lambda} \mid s_0, \boldsymbol{\Lambda}_0 \stackrel{\text{iid}}{\sim} W(\boldsymbol{\Lambda}_0, s_0)$, where W is a Wishart distribution, with mean $s_0 \boldsymbol{\Lambda}_0$. As customary hyperparameter choice, we set $\boldsymbol{\mu}_0$ to be the K -dimensional vector of 0, $s_0 = K + 2$, $\boldsymbol{\Lambda}_0$ to be a $K \times K$ diagonal matrix with elements on the diagonal being equal to 10, and $\nu_0 = 10$. Elicitation for the latter two parameters is discussed in Supplementary Material A.

4 Bayesian Nonparametric Covariate Driven Clustering

In this section, we introduce the Product Partition Model (PPM) and describe its extension to incorporate the Normalized Generalized Gamma process (NGGP). We follow Müller et al. (2011)'s approach to integrate predictive biomarkers into the model, making the random partition dependent on predictive markers. We devise a covariate-dependent prior on the random partition that enables predictive markers to drive the clustering process. Thereby, we induce clusters of homogeneous observations in terms of predictive biomarkers. The resulting model defines independence across clusters and exchangeability only within clusters. The joint evaluation of prognostic and predictive covariates guides the optimal treatment selection, our main inferential goal. Still, only the predictive markers identify patients likely to benefit from a particular therapy. In this way, we may quantify the extent of benefit offered by a specific treatment on groups of patients characterized by similar values of the predictive markers. We denote with $\mathcal{P}_n := \{S_1, \dots, S_{C_n}\}$ the partition of the data label set $\{1, \dots, n\}$ into C_n subsets S_j , for $j = 1, \dots, C_n$ and with $n_j = |S_j|$ being the cardinality of cluster j . In the seminal paper by Hartigan (1990) the prior on \mathcal{P}_n is assigned by letting

$$p(\mathcal{P}_n) = V_{n, C_n} \prod_{j=1}^{C_n} \rho(S_j), \quad (4.1)$$

where $\rho(\cdot)$ is referred to as cohesion function, and quantifies the unnormalized probability of each cluster (Müller et al., 2011). Moreover, V_{n, C_n} is a normalizing constant assuring that the prior sum up to one over the space of all partitions of the integers $\{1, \dots, n\}$. If $\rho(S_j)$ is only a function of $n_j = |S_j|$, then the resulting model for \mathcal{P}_n is invariant under permutations of the labels of the set of integers $\{1, \dots, n\}$. Under this assumption, the resulting model for \mathcal{P}_n falls in the class of Gibbs-type priors (Gnedin and Pitman, 2006). In this framework, the cohesion assume the analytical expression $\rho(S_j) = (1 - \sigma)_{n_j-1}$ with $\sigma < 1$ and $(1 - \sigma)_{n_j-1}$ being the rising factorials, defined as $(a)_n = a(a+1) \dots (a+n-1)$, with $(a)_0 = 1$; $p(\mathcal{P}_n)$ is denoted as *exchangeable partition probability function* (eppf) and the normalizing constant V_{n, C_n} must satisfy the triangular recursion $V_{n, C_n} = V_{n+1, C_n}(n - \sigma C_n) + V_{n+1, C_n+1}$ for each $n > 1$ and $1 \leq k \leq n$ with the proviso that $V_{1,1} = 1$. Note that, since $\rho(S_j)$ is an increasing function of the cluster size n_j , heavily populated clusters are more likely. This leads to the *rich-get-richer* behaviour in the clustering induced by the BNP prior. The connection between product partition models and Gibbs-type prior has been deeply investigated since the seminal paper by Quintana and Iglesias (2003), see also De Blasi et al. (2013).

In this paper we choose $\sigma \geq 0$ and introduce a new parameter $\kappa > 0$ such that: $V_{n, C_n} = \frac{1}{\Gamma(n)} \int_0^\infty u^{n-1} \exp\{ - (1/\sigma)[(\kappa+u)^\sigma - \kappa^\sigma] \} (\kappa+u)^{-n+\sigma C_n} du$. In this way, the law of \mathcal{P}_n coincides with the one induced by the Normalized generalized gamma process (NGGP, Lijoi et al., 2007). The NGGP encompasses the well known Dirichlet process (DP) when $\sigma = 0$. In particular, Lijoi et al. (2007) highlighted the role of σ in the *predictive mechanism* of an NGGP: $p(\tilde{\boldsymbol{\eta}} \in \cdot \mid \mathcal{P}_n, \boldsymbol{\eta}_1^*, \dots, \boldsymbol{\eta}_{C_n}^*) = \frac{V_{n+1, C_n+1}}{V_{n, C_n}} G_0(\cdot) + \frac{V_{n+1, C_n}}{V_{n, C_n}} \sum_{j=1}^{C_n} (n_j - \sigma) \delta_{\boldsymbol{\eta}_j^*}$. The above formula describes the rule used to assign a new observation to a cluster, where the summand on the left represents the probability of forming a new group, and the one on the right represents the probability of being assigned to an already observed

group. It is apparent that larger values of σ increase the probability of generating new groups. From our simulation study (Supplementary Material B.1; see also Lijoi et al., 2007, Section 3.2) large values of σ also reduce the number of estimated singletons. These behaviours result in mitigating the rich-get-richer property of BNP priors. We also assume a discrete prior distribution for (κ, σ) . In this way, we let the data choose the appropriate reinforcement rate (Lijoi et al., 2007), and we overcome a critical “trade-off” occurring when κ and σ are set to a fixed value. Indeed, both the parameters σ and κ have an effect on the number of clusters C_n and on the reinforcing mechanism (see Lijoi et al., 2007; Favaro et al., 2013; Argiento et al., 2016, for a deep discussion). We mention that both have an increasing effect on the probability of observing a new cluster and the prior (and posterior) number of clusters. Interestingly, σ also enters the expression of the weights of existing clusters and, as observed before, reduces the probability of clusters with few elements. We refer to this double effect of σ as the “trade-off” between the number of clusters and reinforcement. In particular, for (κ, σ) we adopted a discrete prior on a 10×10 grid in $(0, 15) \times (0.0, 0.6)$, such that the marginal distribution are discrete approximation of $\kappa \sim \text{Gamma}(2, 1)$ and $\sigma \sim \text{Beta}(5, 23)$, respectively. Extending the work by Müller et al. (2011), we aim at obtaining a prior for the random partition that encourages two subjects to co-cluster when they have similar covariates, i.e., predictive biomarkers. In particular, the prior on the random partition is defined perturbing the cohesion function of a product partition model in equation (4.1) via a similarity function g inducing the desired dependence on covariates. More in detail, the *similarity* function g is a non-negative function that depends on the covariates associated with subjects in each cluster. Let \mathbf{x}_i denote the covariates for the i -th unit, while $\mathbf{x}_j^* = (\mathbf{x}_i, i \in S_j)$ represents the covariates arranged by cluster. The product partition distribution with covariates is

$$p(\mathcal{P}_n) \propto V_{n, C_n} \prod_{j=1}^{C_n} \rho(n_j) g(\mathbf{x}_j^*). \quad (4.2)$$

The choice of the similarity function is of paramount importance for our modeling. It measures the homogeneity of covariates arranged by clusters, and thus, the more the covariates take similar values, the larger the value of g must be. The default choice, proposed by Müller et al. (2011), defines g as the marginal probability of an auxiliary Bayesian model. Several alternatives can be taken (see for example Page and Quintana, 2018; Argiento et al., 2022), since the only requirement for g is to be a symmetric non-negative function. We implement the “Double Dipper” similarity function because it has been shown to work well both in settings with a large number of covariates and in settings where prediction is the main inferential goal (Page and Quintana, 2016, 2018):

$$g(\mathbf{x}_j^*) = \prod_{q=1}^Q \int \prod_{i \in S_j} p(x_{iq} | \xi_j^*) p(\xi_j^* | \mathbf{x}_{jq}^*) d\xi_j^*, \quad (4.3)$$

with $p(\xi_j^* | \mathbf{x}_{jq}^*) \propto \prod_{i \in S_j} p(x_{iq} | \xi_j^*) p(\xi_j^*)$. This structure is not due to any probabilistic properties since the covariates are not considered random, but it measures the similarity of the covariates in cluster S_j . The name comes from the fact that the covariates are used twice and correspond to the \mathbf{x}_j^* ’s posterior predictive. The model in equation (4.3) is completed by assuming $p(\cdot | \xi_j^*) = N(\cdot | m_j^*, v_j^*)$, where $N(\cdot | m, v)$ is a Gaussian density with mean m and variance v , and $p(\xi_j^*) = p(m_j^*, v_j^*) = \text{NIG}(m_j^*, v_j^* | m_0, k_0, v_0, n_0)$ is the Normal-Inverse-Gamma density function. The resulting similarity function can model scenarios with heterogeneous within-cluster variability. We follow Page and Quintana (2018) and set the parameters of the Normal-Inverse-Gamma density to the default values $m_0 = 0, k_0 = 1.0, v_0 = 1.0, n_0 = 2$; since there is no notion of the \mathbf{x}_i being random, parameters ξ_j^* are not updated. Approaches based on covariate-dependent random partition perform well if the clustering is not completely driven by covariates. As the number of covariates increases, similarity functions tend to overwhelm the information provided by the response, completely driving the clustering process. To counteract this behavior, we calibrate the influence of covariates on clustering. To this end, with an abuse of notation, g in equation (4.2) is taken to be $g(\mathbf{x}_j^*) := g(\mathbf{x}_j^*)^{1/\sqrt{Q}}$, namely a small variation of the *coarsened similarity* function by Page and Quintana (2018). The impact of the cohesion and similarity functions on the number of clusters is evaluated in a simulation study reported in Supplementary Material B; in summary, this simulation study demonstrates the effectiveness of the NGGP in controlling the prior mass allocated to different partitions through the reinforcement mechanism induced by σ . Additionally, we observe that the covariates included in the prior effectively drive the clustering process, as desired.

5 Posterior Inference and Treatment Selection

We implement an MCMC algorithm to simulate from the posterior distribution of the parameters of interest. The core part of the MCMC algorithm is the update of cluster membership; the computation associated with the joint law of $(\mathcal{P}_{n^a}^a, \boldsymbol{\eta}_j^{a*})$ is based on Neal (2000)’s Algorithm 8 with a reuse strategy (Favaro et al., 2013). Conditional on the updated cluster labels, all the remaining parameters are easily updated with Gibbs sampler or Metropolis-Hastings

steps. Details on posterior inference are given in Supplementary Material C. To perform treatment selection for a new untreated patient, we need to predict the treatment outcome under each competing treatment \tilde{y}^a , for $a = 1, \dots, T$. Given the observed responses \mathbf{y}^a for the n^a patients previously treated with therapy a , the predictive probability of response level k under treatment a is $p(\tilde{y}^a = k \mid \mathbf{y}^a, \mathbf{z}^a, \mathbf{x}^a, \tilde{\mathbf{z}}, \tilde{\mathbf{x}})$, where $\tilde{\mathbf{z}}$ and $\tilde{\mathbf{x}}$ denote the new patient's biomarkers. We establish utility weights that turn a multinomial setting into a one-dimensional selection criterion considering the relative importance of each level of the ordinal response. Let $\boldsymbol{\omega} = (\omega_1, \dots, \omega_K)^\top$ be a K -dimensional vector denoting the utility assigned to tumor response levels. We can then compute the median predictive utility for a new patient treated with treatment a as $\tilde{\varphi}(a, \boldsymbol{\omega}, \mu_{0.5}) = \sum_{k=1}^K \omega_k \mu_{0.5}(\tilde{y}^a = k \mid \mathbf{y}^a, \mathbf{z}^a, \mathbf{x}^a, \tilde{\mathbf{z}}, \tilde{\mathbf{x}})$, where $\mu_{0.5}(\cdot)$ denotes the median of the posterior predictive distribution; see Supplementary Material C.3 for more details. The approach under consideration may not be suitable for complex settings where treatment selection depends on assessing multiple endpoints. Lee et al. (2022) suggest an alternative approach that involves eliciting a utility function dependent on both covariates and response to account for two endpoints. Finally, an untreated patient will be assigned to the treatment with the highest predicted utility.

6 Simulation Study

We carried out a comparative study on simulated data to evaluate the performance of our method. We compare the proposed integrative model for personalized treatment selection (t-ppmx) with the two-step predictive model proposed by Ma et al. (2019) using, for the first step, three alternative clustering procedures, namely K-means (km-bp), Partitioning Around Medoids (pam-bp) and Hierarchical Clustering (hc-bp). T-ppmx is also compared with a selection rule based on Dirichlet-multinomial (DM) regression model. We assume a horseshoe prior on the regression coefficients for a fair comparison. In the DM regression model, we included the main effects of prognostic and predictive biomarkers and all the interaction terms between predictive covariates and the treatment. We fit the models on the n_{train} patients of the training set, and we evaluate the predictive performance on n_{test} patients in the test set. The approach proposed by Ma et al. (2019) employs the Consensus Clustering method (Monti et al., 2003), which determines clustering for a specified number of clusters C . Since the number of groups is unknown, C must be selected using leave-one-out cross-validation for each simulated patient. Note that this is not true for our approach, and our method does not need to perform this extra step. We generate simulated datasets closely following the strategy devised in Ma et al. (2019), i.e., we do not employ our model as the generative mechanism. The patients are assigned to $T = 2$ treatments, and $K = 3$ levels of the response variable are considered. Since the observed treatment endpoints were unavailable, the treatment response and the optimal treatment for each simulated patient were generated. In particular, we set $\boldsymbol{\omega} = (0, 40, 100)^\top$ to make the ordinal response reflect the clinical importance of each level; additional details on the data generating mechanism and on the weights elicitation are provided in Supplementary Material D and A, respectively.

6.1 Performance evaluation

Prediction performances are compared in terms of the following metrics:

- (i) *MOT*: it counts the number of patients misassigned to their optimal treatment;
- (ii) $\% \Delta MTU$: it measures the relative gain in treatment utility;
- (iii) *NPC*: it counts the number of patients whose outcome has been correctly predicted.

The true optimal treatment for each simulated patient is available since has been determined as a result of the generating mechanism. *MOT* represents a first measure to compare the methods, its interpretation is straightforward, and lower values are associated with better selection rules. Nonetheless, the extent to which a particular treatment is beneficial for each patient is heterogeneous, and the improvement offered by a therapy varies from patient to patient. The relative gain in Treatment Utility (Ma et al., 2016), $\% \Delta MTU$, measures the overall benefit ensured by a treatment selection rule in the case of $T = 2$ competing treatments. In particular, $\% \Delta MTU$ is bounded above by 1 when it always recommends the optimal treatment, and $\% \Delta MTU = -1$ when it fails to select the optimal therapy for all the patients. More details on this measure can be found in Supplementary Material E. The *NPC* metric represents the number of patients whose outcome is correctly predicted.

6.2 Simulation scenarios and results

Methods are compared on scenarios of increasing complexity. We construct Scenarios 1a and 1b following the generating mechanism described in Supplementary Material D, using 2 prognostic and 25 and 50 predictive biomarkers, respectively. Other scenarios emulate the pronounced heterogeneity that genomics data feature. Namely, the predictive covariates employed to generate the response differ in the train and the test set since they overlap only to some extent.

Table 1: Predictive performance: mean across 50 replicated datasets, standard deviations are in parentheses. In each scenario and for each index, the best performance is in bold.

	Scenario 1a			Scenario 1b		
	<i>MOT</i>	<i>%ΔMTU</i>	<i>NPC</i>	<i>MOT</i>	<i>%ΔMTU</i>	<i>NPC</i>
pam-bp	14.0600 (3.2351)	0.0192 (0.3447)	10.2600 (1.9672)	14.2400 (2.9593)	-0.0106 (0.3429)	13.2000 (2.2039)
km-bp	13.4200 (2.8074)	0.1130 (0.3038)	11.4000 (2.5314)	13.4000 (2.6108)	0.0750 (0.3076)	13.9600 (2.2584)
hc-bp	12.8600 (3.1429)	0.1520 (0.3642)	12.0200 (2.8961)	12.4400 (3.1374)	0.1418 (0.3403)	12.6800 (2.7807)
dm-int	12.6000 (3.4934)	0.1756 (0.3536)	13.8200 (2.9877)	13.2800 (3.7310)	0.0740 (0.3851)	12.9600 (3.0902)
t-ppmx	10.0000 (3.2451)	0.3933 (0.3080)	15.1600 (2.2800)	10.7800 (3.2968)	0.3339 (0.3362)	14.4280 (2.8646)
	Scenario 2a			Scenario 2b		
	<i>MOT</i>	<i>%ΔMTU</i>	<i>NPC</i>	<i>MOT</i>	<i>%ΔMTU</i>	<i>NPC</i>
pam-bp	14.1600 (3.2474)	0.0145 (0.3405)	10.1600 (2.2439)	14.2000 (2.9966)	-0.0068 (0.3487)	13.2200 (2.2341)
km-bp	13.3600 (2.9190)	0.1136 (0.3082)	12.4800 (2.7198)	13.5200 (2.5414)	0.0689 (0.3037)	13.7800 (2.2883)
hc-bp	12.9600 (3.5165)	0.1223 (0.3846)	11.5400 (11.54)	12.4400 (3.1112)	0.1430 (0.3344)	12.7600 (2.7372)
dm-int	12.9600 (3.5165)	0.1223 (0.3847)	11.5400 (2.8082)	13.0400 (3.5798)	0.1021 (0.3627)	13.0200 (2.9657)
t-ppmx	10.6200 (3.3313)	0.3578 (0.3347)	15.3800 (2.5446)	10.6000 (3.1880)	0.3497 (0.3269)	14.4400 (2.8224)
	Scenario 3a			Scenario 3b		
	<i>MOT</i>	<i>%ΔMTU</i>	<i>NPC</i>	<i>MOT</i>	<i>%ΔMTU</i>	<i>NPC</i>
pam-bp	13.9800 (3.3654)	0.0275 (0.3469)	11.8600 (2.6955)	14.5000 (2.9433)	-0.0635 (0.3310)	14.1400 (2.8856)
km-bp	13.3600 (2.8909)	0.1159 (0.3055)	11.6000 (2.6954)	13.7000 (2.9014)	0.0405 (0.3363)	13.8000 (2.5873)
hc-bp	12.6600 (3.2740)	0.1621 (0.3684)	11.5000 (2.8158)	12.9800 (3.3715)	0.0859 (0.3647)	12.3800 (2.3724)
dm-int	12.7400 (3.7461)	0.1616 (0.3747)	13.9000 (3.1445)	12.8400 (3.1646)	0.0957 (0.3548)	13.6000 (2.9207)
t-ppmx	10.2600 (3.6411)	0.3610 (0.3352)	15.0400 (2.4320)	10.8600 (3.1234)	0.3244 (0.3281)	14.8400 (2.6677)

The pairs of scenarios (2a, 2b) and (3a, 3b) match (1a, 1b) in the number of predictive covariates, but predictive markers employed to generate the response in the train and test set overlap at 90% and 80%, respectively. Train and test sets consist of 124 and 28 observations, respectively. Scenarios with 25 covariates are labeled with “a”, while those with 50 covariates with “b”. Hyperparameters are set to the default values given in the previous sections; sensitivity to these settings is studied in Supplementary Material A. We run the algorithm for 12,000 iterations, with a burn-in period of 2,000 iterations; chains were thinned, and we kept every 5–th sampled value. We fit the model on 50 replicated datasets. Reported values are averaged over the replicated datasets, with standard deviations in parentheses.

Overall, t-ppmx outperforms all competing methods (Table 1). This result can be attributed to the ability of the covariate-dependent random partition to reach significant clustering arrangements. Among the two-stage methods, pam-bp consistently exhibits inferior performance compared to other methods, at least considering MOT and MTU. While km-bp and hc-bp produce comparable results, hc-bp demonstrates superior performance, especially when the number of covariates is large. However, km-bp exhibits greater robustness to increasing heterogeneity, at least for moderate numbers of covariates, and deteriorates less compared to hc-bp. Dm-int and hc-bp exhibit similar performance in scenarios with a moderate number of covariates. However, as the number of covariates increases, dm-int demonstrates greater robustness. Conversely, hc-bp shows superior robustness in scenarios with considerable hetero-

geneity. Interestingly, t-ppmx is robust with respect to increasing heterogeneity. It is probably due to the integrated prediction mechanism, which fully accounts for the uncertainty in the clustering; note that, for the proposed method, optimal treatment misassignment often pertains to patients with similar utility across treatments. Our simulation study suggests that t-ppmx should be preferred over two-step methods. In this simulation study, no measure of clustering accuracy has been produced since the generative mechanism for synthetic data implies that no “true” clustering exists. To evaluate the clustering performances of t-ppmx, we design three scenarios where covariates have a known intrinsic data structure, and clustering explicitly depends on covariates. This enables us to compare PPMx’s posterior partition with the true one. In Supplementary Material B we compare the methods on alternative scenarios to examine their robustness across different generating processes, and we also assess the impact of misspecification of prognostic and predictive covariates on t-ppmx’s clustering and predictive performances.

7 Case Study of Low-grade Glioma

Glioma is the most frequent brain tumor: it makes up approximately 30% of all brain and central nervous system tumors and 80% of all malignant brain tumors (Goodenberger and Jenkins, 2012). Gliomas are classified as grades I to IV based on histological criteria established by the World Health Organization (WHO). Grade I tumors are generally circumscribed benign tumors with favorable prognoses, while grades II-IV comprise more aggressive tumors (diffuse gliomas). Grade II and grade III gliomas are usually referred to as low-grade glioma (LGG), which may eventually progress to grade IV, high-grade glioma. Most LGG patients undergo resection and then receive radiotherapy and/or chemotherapy. Nonetheless, these standard procedures have proved to be largely inadequate (Claus et al., 2015). LGG exhibits significant molecular heterogeneity, and many research efforts are now devoted to developing precision medicine for these patients (Olar and Sulman, 2015; Ius et al., 2018). We apply our method to the dataset analyzed in Ma et al. (2019), where clinical data and protein expression of patients affected by lower-grade glioma are collected from the TCGA data portal (<https://portal.gdc.cancer.gov/>, accessed August 31, 2023). Publicly available data underwent an accurate preprocessing, thoroughly documented in Ma et al. (2019), and summarized in Supplementary Material F. The resulting LGG dataset comprises patients that received standard and advanced treatments. A treatment qualifies as advanced if it includes targeted therapies or radiotherapy. Each group comprises 79 patients balanced in the covariates to account for potential selection bias. Following Ma et al. (2019), we defined the tumor response for the LGG dataset using the RECIST criteria (<http://www.recist.com/>, accessed August 31, 2023). In our analysis, tumor response is formulated in three ordinal levels: progressive disease (PD), partial response/stable disease (PS), and complete response (CR). Utility weights for treatment selection for ordinal outcomes are elicited. Namely, $\omega = (0, 40, 100)^\top$ to make the ordinal response reflect the clinical importance of each level (Ma et al., 2016). We evaluate the robustness of our method to weight elicitation in Supplementary Material I. Finally, we analyze the same 23 predictive and 2 prognostic protein expressions considered in Ma et al. (2019). See Supplementary Material F for more details, including the list of predictive and prognostic proteins. TCGA data do not provide the true optimal treatment, and only the NPC measure, among those discussed in Section 6.1, can be used. We employ an empirical summary measure (ESM, Song and Pepe, 2004) to evaluate the relative increase in the population response rate attributable to a treatment allocation method compared to random allocation. Let Y be the binary outcome variables, taking 0 for non-respondents or 1 for respondent patients. We define the treatment contrast as $\Delta(\mathbf{X}, \mathbf{Z}) = Pr(Y = 1|A = 2, \mathbf{X}, \mathbf{Z}) - Pr(Y = 1|A = 1, \mathbf{X}, \mathbf{Z})$, where $A = \{1, 2\}$ denote the non-targeted and targeted treatment, respectively. Indicating with $Pr(Y = 1|A_r)$ the probability of being a respondent under a randomized treatment assignment, we obtain the relative increase in the population response rate under a personalized treatment selection rule as: $ESM = \{Pr(Y = 1|A = 2, \Delta(\mathbf{X}, \mathbf{Z}) > 0) \times Pr(\Delta(\mathbf{X}, \mathbf{Z}) > 0) + Pr(Y = 1|A = 1, \Delta(\mathbf{X}, \mathbf{Z}) < 0) \times Pr(\Delta(\mathbf{X}, \mathbf{Z}) < 0)\} - Pr(Y = 1|A_r)$, see Supplementary Material E for more details. Note that we based this summary measure on only two response categories, responders (CR) and non-responders (PD + PS), whereas we used all three levels of the ordinal outcome in the data analysis and to implement personalized treatment selection.

7.1 Results

In this section, we applied the proposed method to the LGG dataset alongside the approach proposed by Ma et al. (2019). Table 2 reports NPC and ESM summary measures computed from assignments obtained using a 10-fold cross-validation strategy. We run the algorithm for 12,000 iterations, with a burn-in period of 2,000 iterations; chains were thinned, and we kept every 5-th sampled value. We report MCMC diagnostic checks in Supplementary Material F. The proposed t-ppmx outperforms competing methods both in terms of NPC and ESM. These results are consistent with those obtained in our simulations studies, especially in scenarios featuring significant heterogeneity and a moderate number of predictive covariates (Scenarios 2a and 3a). In particular, t-ppmx attains an ESM of 0.1008, while ESM for pam-bp is 0.0553 among two-stage procedures. Patients show pronounced heterogeneity, particularly

Table 2: Predictive performance: metrics are obtained gathering 10-fold cross-validation results. For each index, the best performance is in bold.

	NPC	ESM
pam-bp	48	0.0553
km-bp	45	0.0384
hc-bp	48	0.0285
dm-int	64	0.0746
t-ppmx	69	0.1008

those assigned to Treatment 2. The absence of a sharp separation between clusters demonstrates a significant uncertainty in the clustering. Patients assigned to Treatment 1 form more homogeneous clusters, but the low probability of co-clustering still indicates a large variability in clusters' assignments.

7.2 Cluster Analysis

Here, we want to investigate the composition of the clusters identified to characterize the profiles of co-clustered patients. Following [Wade and Ghahramani \(2018\)](#), we use the variation of information loss function to estimate the

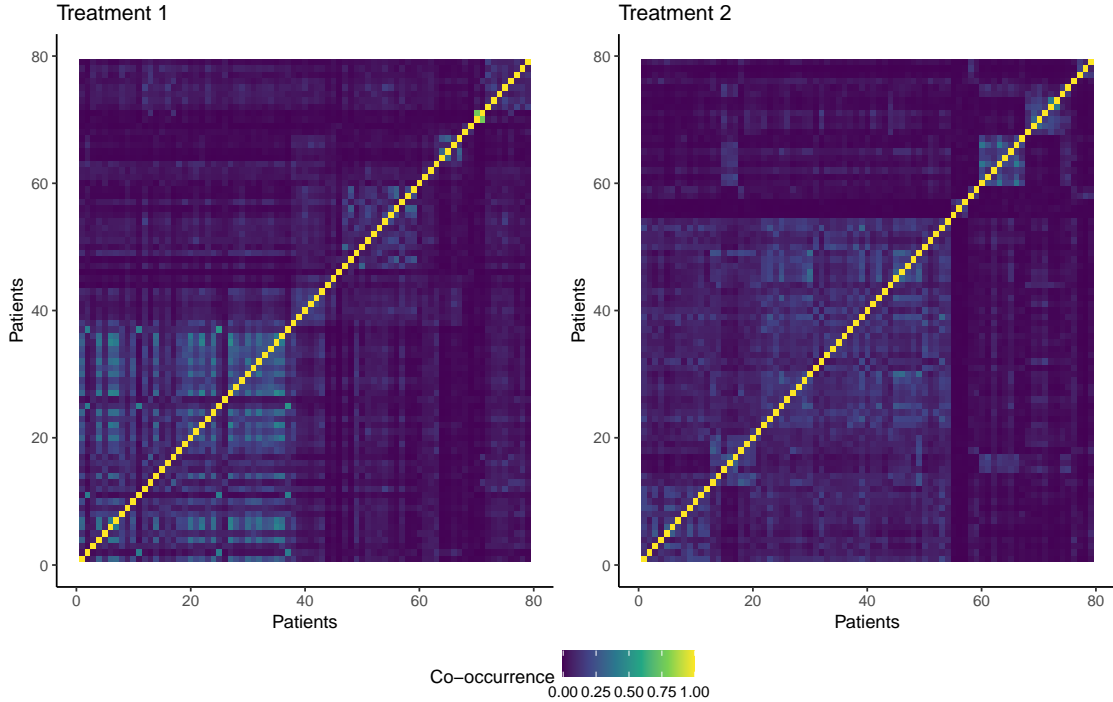


Figure 1: Heatmap of averaged co-occurrence matrix for patients that received Treatment 1 (left) and Treatment 2 (right).

optimal partition on the space of clusters. In particular, we obtain a partition of the 79 patients that received the *standard treatment* (Treatment 1) into 10 groups ranging from 1 to 38. Similarly, patients that received the *advanced treatment* (Treatment 2) are grouped into 10 clusters with cluster membership ranging from 1 to 34. Figure 1 reports the heatmap of the averaged co-occurrence matrices. We refer to T1G1, ..., T1G10 to denote the groups of patients treated with the standard treatment (left panel of Figure 1) and to T2G1, ..., T2G10 for the groups of patients that received the advanced treatment (right panel). Our PPMx model provides homogeneous clusters in terms of predictive covariates; indeed, it substantially reduces the within-group variance for each predictive covariate (see Figure 4 in Supplementary Material G). We deem clusters with less than 8 members residual clusters and exclude them from the following analysis. To characterize the groups, we consider the cluster-specific mean for predictive biomarkers. Figure 2 shows that cluster-specific means in T1G2, T1G4, and T2G6 strongly depart from the population value. Moreover, T1G2 and

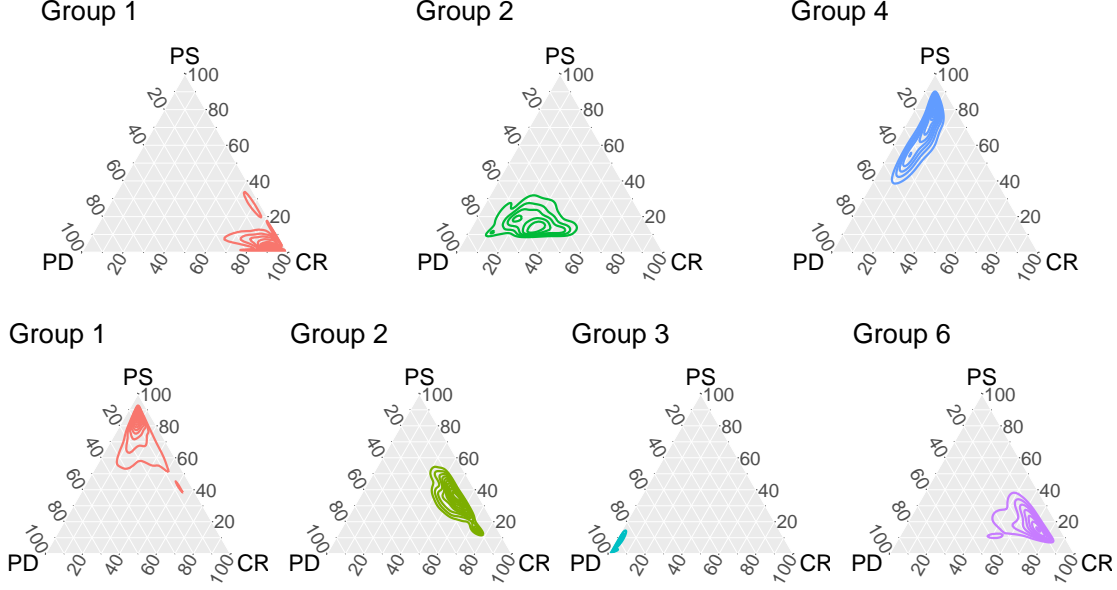


Figure 3: Ternary plot of the posterior density of group-specific response probabilities for patients that received Treatment 1 (first row) and Treatment 2 (second row).

8 Discussion

We have proposed a novel Bayesian approach that, given a set of predictive and prognostic biomarkers, suggests the best-suited treatment for each patient. The model clusters patients into homogeneous groups with respect to their predictive markers, separately for each treatment. Cluster-level effects adjust the baseline probability of response to treatment obtained by prognostic factors. As a key innovative feature of the proposed approach, model-based clustering and treatment assignment are jointly estimated from the data, that is, treatment selection fully accounts for patients' heterogeneity. Simulation studies and the analysis of LGG data showed that the proposed method is well suited for predictions in scenarios of practical relevance, e.g., in the presence of considerable heterogeneity. Moreover, our approach leads to a precise characterization of the clusters of patients supported by the data, identifying the group of patients more likely to benefit from targeted treatments. In its current version, the model is designed to be used after the biomarker discovery phase, i.e., after identifying relevant prognostic and predictive biomarkers. This limitation could be addressed by adopting variable selection approaches in the Bayesian framework. Nevertheless, while the use of the latter methods is straightforward when selecting prognostic biomarkers entering the likelihood, variable selection methods for product partition models are part of our ongoing research (see for instance [Barcella et al., 2017](#)). In this regard, we would like to highlight that, although assuming which are the prognostic and predictive biomarkers may be restrictive in certain scenarios, and we could recast the proposed model to accommodate this lack of knowledge, this assumption remains practically very relevant. In fact, the major drawback of a model that simultaneously performs biomarker discovery and treatment selection would be the absence of a confirmatory process. Biomarkers can lead to targeted therapy and serve as useful prognostic and predictive factors of clinical outcomes. Nonetheless, biomarkers need to be validated on a completely independent data set not used during development to serve these purposes.

Acknowledgements

We thank J. Ma for providing us with the companion R code of [Ma et al. \(2019\)](#). The first and third authors were partially supported by the “Dipartimenti Eccellenti 2023-2027” ministerial funds (Italy). All authors were partially supported by grant “CLustering: Bayesian Partition Models for Precise Medicine (CluB: PMx²)”, funded by *Fondo di Beneficienza di Intesa San Paolo* (Italy), the last author was partially supported by the Tuscany Health Ecosystem (THE) grant, funded by *Ministero dell’Università e della Ricerca*.

Supporting Information

The R code is also available on GitHub: <https://github.com/mattpedone/treatppmx>. Results and Figures can be reproduced using the scripts available at <https://github.com/mattpedone/Reproduce-tPPMx>.

A Sensitivity Analysis

A.1 Hyperparameter settings

Our predictive model involves some hyperparameters that require careful tuning. To this end, we investigate the sensitivity of the results to these values. In particular, we construct the sensitivity study on Scenario 1a presented in Section 7.3, which considers 25 predictive and 2 prognostic biomarkers. Also, in Scenario 1a, we assign 152 patients to 2 competing treatments, and $K = 3$ levels of the ordinal response are assumed. We adopt a train and test strategy.

For different specifications of parameters ν_0 and Λ_0 , we evaluate the model's performance in terms of prediction, goodness-of-fit, and clustering production. In particular, we assume that Λ_0 is a diagonal matrix, and we evaluate the sensitivity of the results to their specification over the following grid of values: (i) $\nu_0 = \{0.1, 1.0, 10.0\}$; (ii) $\Lambda_{0_{kk}} = \{0.1, 1.0, 10.0\}$; for $k = 1, \dots, K$.

To assess treatment selection performance, we use the summary measures discussed in Section 7.2. We also report the log-pseudo-marginal-likelihood (*lpml*), a goodness-of-fit metric (Christensen et al., 2011) that accounts for model complexity. Finally, to take into consideration also the cluster arrangement produced, we report the variation of information (*VI*, Wade and Ghahramani, 2018).

We run the algorithm for 12,000 iterations, with a burn-in period of 2,000 iterations; chains are thinned, and we keep every 5-th sampled value. The analysis of each configuration is replicated, and the results averaged over 50 runs, with standard deviations in parentheses. Results are reported in Tables A1 and A2. In Tables A1 and A2, $\{\Lambda_{0_{kk}}\}$ denote the set of K elements on the diagonal of Λ_0 . Since clustering is performed independently across treatments, results are reported separately for each treatment. In Table A2, T1 and T2 refer to Treatment 1 and Treatment 2, respectively. We recall that the generative mechanism for synthetic data presented in Section 7.1 implies that no "true" clustering exists. Consequently, we can not establish the best performance in terms of clustering production.

		$\nu_0 = 0.1$		$\nu_0 = 1.0$		$\nu_0 = 10.0$	
$\{\Lambda_{0_{kk}}\} = 0.1$	<i>MOT</i>	10.4400	(4.1264)	10.4800	(3.5181)	10.9800	(3.5021)
	<i>%ΔMTU</i>	0.3631	(0.4298)	0.3507	(0.3518)	0.3359	(0.3498)
	<i>NPC</i>	14.9400	(2.5826)	14.7400	(2.5299)	15.5000	(2.0727)
	<i>lpml</i>	-90.21869	(16.5508)	-87.8940	(9.2803)	-86.9153	(11.2025)
$\{\Lambda_{0_{kk}}\} = 1.0$	<i>MOT</i>	10.7400	(3.3124)	10.1200	(3.5722)	10.2200	(3.0257)
	<i>%ΔMTU</i>	0.3391	(0.3433)	0.3946	(0.3381)	0.4121	(0.2785)
	<i>NPC</i>	15.1600	(2.2620)	15.2200	(2.5737)	15.4400	(2.2054)
	<i>lpml</i>	-88.5130	(14.5700)	-87.1011	(12.8265)	-90.3171	(13.2682)
$\{\Lambda_{0_{kk}}\} = 10.0$	<i>MOT</i>	10.6800	(3.1197)	10.3300	(3.4890)	10.0000	(3.2451)
	<i>%ΔMTU</i>	0.3485	(0.3071)	0.3913	(0.3455)	0.3933	(0.3080)
	<i>NPC</i>	14.6800	(2.3599)	15.2000	(2.7701)	15.1600	(2.2800)
	<i>lpml</i>	-88.4072	(13.2897)	-86.4222	(10.7379)	-86.4955	(10.9973)

Table A1: Predictive and goodness-of-fit performance: mean across 50 replicated datasets, standard deviations are in parentheses. For each index the best performance is in bold.

		$\nu_0 = 0.1$		$\nu_0 = 1.0$		$\nu_0 = 10.0$	
		T1	T2	T1	T2	T1	T2
$\{\Lambda_{0_{kk}}\} = 0.1$	<i>VI</i>	7.6000 (0.8330)	8.0000 (0.0000)	7.7000 (0.5440)	8.000 (0.0000)	7.2000 (1.0498)	8.0000 (0.0000)
	<i>VI</i>	7.6200 (.6966)	7.9600 (0.1979)	7.3800 (0.8781)	8.0000 (0.0000)	7.4200 (0.8104)	7.9800 (0.1414)
$\{\Lambda_{0_{kk}}\} = 1.0$	<i>VI</i>	7.4600 (0.8855)	8.0000 (0.0000)	7.5400 (0.9091)	8.0000 (0.0000)	7.4600 (0.9304)	8.0000 (0.0000)
	<i>VI</i>	7.4600 (0.8855)	8.0000 (0.0000)	7.5400 (0.9091)	8.0000 (0.0000)	7.4600 (0.9304)	8.0000 (0.0000)

Table A2: Cluster production performance: mean across 50 replicated datasets, standard deviations are in parentheses.

The results are robust to different hyperparameter specifications, and we do not observe any sensitivity of the result to the values' specification. In the simulation study and the case study reported in the paper, we set $\{\Lambda_{0_{kk}}\} = 10.0$, and $\nu_0 = 10.0$.

A.2 PS weights elicitation

Following Ma et al. (2019), the weight assigned to the partial response/stable disease (PS) was determined using a utility-based criterion, to take into consideration its clinical importance. Weights were given on a scale of 0 to 100, with 0 being the least favorable response level and 100 being the most favorable response level ($\omega_0 = 0$ and $\omega_K = 100$). The weight for the intermediate response level (PS) was determined based on its benefit in terms of long-term overall survival duration, estimated through a Cox regression model, as recommended by Ma et al. (2016). A landmark analysis was performed over a period of 120 days, given that a significant proportion of the observed responses occurred subsequent to the completion of two consecutive eight-week treatment cycles. Specifically, the estimated relative risk of 10-year overall survival for response level PS was 2.46 when adjusted for age, gender, tumor grade, and initial year of pathological diagnosis (IYPD), with complete response (CR) as the reference. As a result, the utility weight for PS was defined as $(1/2.46)100 \approx 41$. While the weights were not entirely arbitrary, we acknowledge that there may be alternative weighting schemes that could be considered, and to check the robustness of our method, we conducted a sensitivity study in which we varied the weight for PS, $\omega_{PS} = \{20, 40, 60, 80\}$, and re-analyzed the data. The results are displayed in Table A3.

	$\omega_{PS} = 20$		$\omega_{PS} = 40$		$\omega_{PS} = 60$		$\omega_{PS} = 80$	
<i>MOT</i>	11.2200	(2.2614)	10.0000	(3.2451)	7.7600	(5.3321)	6.1800	(4.8051)
% ΔMTU	0.3395	(0.2441)	0.3933	(0.3080)	0.5621	(0.3732)	0.6542	(0.3629)

Table A3: Predictive performance: mean across 50 replicated datasets, standard deviations are in parentheses.

Our sensitivity analysis revealed that the treatment selection is sensitive to the weight elicited for PS. However, we have provided strong and valid justifications for our weight elicitation approach, which we consider to be conservative. In fact, we have observed that setting $\omega_{PS} = 0.40$ may have actually underestimated the true performance of our method, rather than overestimating it. Despite the sensitivity of our results to the weight elicitation method, we believe that our justifications provide a reasonable degree of confidence in the reliability of our findings.

B Additional Simulation Studies

To further assess the performances of our proposed method, we conduct additional simulation studies. These simulations have multiple purposes: (i) to study the effect of the proposed cohesion and similarity functions on the number of induced clusters (Section B.1); (ii) to test the method’s robustness under a different generating process (Section B.2); (iii) to evaluate the method’s ability to recover true clustering structure in the data (Section B.3); (iv) to assess the method’s robustness to misspecification of prognostic/predictive biomarkers (Section B.4).

B.1 Induced prior distribution of the number of clusters

In this section, we empirically verify that our non-parametric prior has the features needed for our application. We argue that the Normalized Generalized Gamma process (NGGP) controls the prior mass allocated to different partitions through the reinforcement mechanism induced by σ . Moreover, we expect the incorporation of covariates in the prior to effectively drive the clustering process. These advantages can be appreciated by evaluating the induced prior distribution on the number C_n of clusters. In order to assess the advantages offered by our covariate-dependent prior for random partitions, we consider a simple comparative example. To this end, we compare the prior distribution on the number of clusters implied by different models for the random partition. Namely, subsequent case (v) coincides with equation 6 in the paper (i.e. the prior adopted in this paper), while experiments (i)-(iv) are relevant sub-cases of (v):

- (i) $\rho(n_j) = \kappa(n_j - 1)!$ and $g \equiv 1$, that yields to a product partition distribution coinciding with the eppf induced by a DP; we will refer to this as DP in the following;
- (ii) $\rho(n_j) = (1 - \sigma)_{n_j}$ and $g \equiv 1$, that yields to a product partition distribution coinciding with the eppf induced by an NGGP; we will refer to this as NGGP in the following;
- (iii) $\rho(n_j) = \kappa(n_j - 1)!$ and g defined as $g(\mathbf{x}_j^*) = g(\mathbf{x}_j^*)^{1/\sqrt{Q}}$, that yields a product partition distribution with covariates with calibrated similarity and whose cohesion coincides with the eppf induced by a DP; we will refer to this as DP-sim in the following;

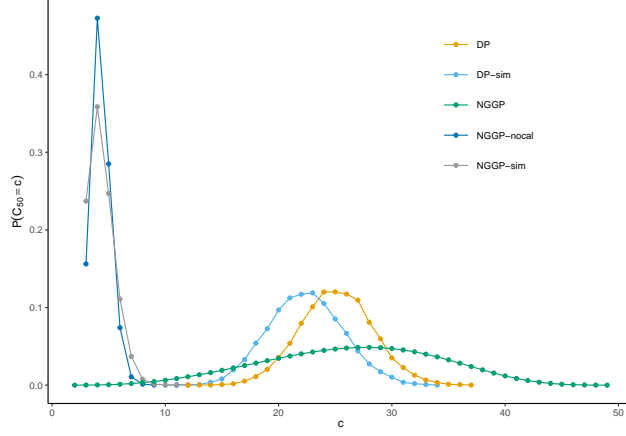


Figure 4: Prior distributions on the number of clusters corresponding to the 5 priors considered.

Table A4: Average number of clusters and proportion of singletons corresponding to the 5 priors considered.

	DP	DP-sim	NGGP	NGGP-nocal	NGGP-sim
Av. # clusters	25.09	22.38	26.25	4.32	4.38
% singletons	55.82%	53.37%	34.45%	9.98%	19.39%

- (iv) $\rho(n_j) = (1 - \sigma)_{n_j}$ and g defined as in equation 7 in the paper, that yields a product partition distribution with covariates with non-calibrated similarity and whose cohesion coincides with the eppf induced by an NGGP; we will refer to this as NGGP-nocal in the following;
- (v) $\rho(n_j) = (1 - \sigma)_{n_j}$ and g defined as $g(\mathbf{x}_j^*) = g(\mathbf{x}_j^*)^{1/\sqrt{Q}}$, that yields a product partition distribution with covariates with calibrated similarity and whose cohesion coincides with the eppf induced by a NGGP; we will refer to this as NGGP-sim in the following;

We fix $n = 50$ and consider the corresponding distributions of the number of components in the five above cases. We set hyperparameters of nonparametric priors such that the prior expected number of clusters, without the effect of the covariates, is $\mathbb{E}(C_{50}) = 25$; specifically, we set $\kappa = 19.2333$ for special cases (i) and (iii), and $\kappa = 0.7353, \sigma = 0.7353$ for (ii), (iv) and (v).

Finally, we generate the covariates from a 3-component mixture of 5-variate normal distributions such that

$$p(\mathbf{x}) = \sum_{j=1}^3 \phi_j N_5(\boldsymbol{\theta}_j, \boldsymbol{\Sigma}),$$

where $\phi = (0.2, 0.5, 0.3)^\top$, $\boldsymbol{\theta}_j$ are 5-dimensional vectors such that $\boldsymbol{\theta}_1 = -2.1\mathbf{1}$, $\boldsymbol{\theta}_2 = \mathbf{0}\mathbf{1}$ and $\boldsymbol{\theta}_3 = 2.3\mathbf{1}$, where $\mathbf{1}$ is the all-ones vector in \mathbb{R}^5 . Finally $\boldsymbol{\Sigma}$ is 5×5 diagonal covariance matrix such that $\boldsymbol{\Sigma} = \text{diag}(0.5, 0.5, 0.5, 0.5, 0.5)$.

As expected, NGGP results in a prior distribution of C_{50} that is rather flat and exhibits a larger variability than the DP-induced distribution. In fact, due to the reinforcement mechanism induced by the σ parameter, the NGGP prior gives *a priori* support to a wider range of the number of clusters, still penalizing the number of singleton partitions (see Table A4). This feature is particularly useful when little is known about the true number of clusters. The PPMx models include information from the covariates, and counteract the misspecification in the prior elicitation of the number of clusters. Nonetheless, when the DP cohesion is adopted, PPMx still does not differ much from the DP, exhibiting a distribution that supports more clusters than the truth. This is due to the rich-get-richer phenomenon, since a large portion of clusters (53%) are singletons, as displayed in Table A4.

Finally, we focus on the PPMx models with NGGP as cohesion function. We consider both the case of calibrated and uncalibrated similarity functions. The implied distributions on the number of clusters give strong support to a moderate number of clusters, in both cases. Nonetheless, when the similarity is not calibrated, the PPMx implies a highly peaked distribution of C_{50} . This phenomenon is consistent with what is observed in Page and Quintana (2018),

where they draw attention to the risk of similarities entirely driving the clustering process. Since this phenomenon is more pronounced for a larger number of covariates (as in our case study), the calibrated similarity is better suited for our application.

In this simulation study we focused our attention on the prior distribution on the number C_n of clusters induced by our prior for random partitions. Experiments (i) and (ii) represent special cases of our covariate-dependent prior, where the covariates do not guide the construction of the partition. DP and the class of Gibbs-type priors (to which NGGP belongs) have been widely studied in the bayesian nonparametric literature. Although we do not aim to provide a comprehensive study of these priors here, we find it interesting to highlight that our results are consistent with the theoretical results obtained by [Lijoi et al. \(2007\)](#) and [De Blasi et al. \(2013\)](#). Furthermore, the following paragraph provides an opportunity to further explain the phenomena of “rich-get-richer” and reinforcement mechanisms mentioned earlier.

As we mention in the manuscript (see Section 4), when the Bayesian nonparametric prior is of Gibbs-type, the cohesion assumes the analytical expression $\rho(S_j) = (1 - \sigma)_{n_j}$ with $\sigma < 1$ and $(1 - \sigma)_{n_j}$ being the rising factorials. It is evident that in this case, $\rho(S_j)$ is an increasing function of the cluster size n_j . So heavily populated clusters are more likely. This phenomenon is named the “rich-get-richer” behaviour of the clustering induced by a nonparametric prior. When $\sigma = 0$, i.e., when the nonparametric prior is the Dirichlet process, the “rich-get-richer” behaviour is quite pronounced. As a consequence, frequently (see also Table A4), the posterior cluster estimate is made by a few very populated clusters and many noisy clusters (i.e. clusters with few elements, or singletons). We refer to [Poux-Médard et al. \(2021\)](#) for a detailed discussion on this.

As shown in our simulation study and discussed in [Lijoi et al. \(2007\)](#); [Favaro et al. \(2013\)](#); [Argiento et al. \(2016\)](#), to mitigate this behaviour, it is convenient to assume $\sigma > 0$ by choosing a Normalized Generalized Gamma process as mixing distribution. In the following we briefly summarize the role of the parameter σ .

Following the notation adopted in the paper, the NGGP is indexed by σ , that controls the clustering, and κ , which plays the role of the mass parameter as in the Dirichlet process, which is recovered when $\sigma = 0$. For detailed discussions on the effects of σ and κ on the prior (and posterior) number of clusters see [Lijoi et al. \(2007\)](#); [Favaro et al. \(2013\)](#); [Argiento et al. \(2016\)](#).

We mention here that the integral defining the V_{n,C_n} in equation (5) depends on κ and σ . Further developing this expression (see [Lijoi et al., 2007](#); [Favaro et al., 2013](#)) it is possible to show that:

- (a) when κ and σ increase, then the prior (and consequently the posterior) mean of C_n increases;
- (b) large values of σ imply heavy tail distribution on the prior for C_n .

Moreover, it is possible to study the effect of κ on the reinforcement mechanism. Indeed, when $\sigma = 0$, i.e. when considering the DP, $\frac{V_{n+1,C_n+1}}{V_{n,C_n}} \propto \kappa$ and $\frac{V_{n+1,C_n}}{V_{n,C_n}} \propto 1$. Then, under the Dirichlet process, increasing κ increases the probability of observing a new cluster. The same behaviour can be deduced when $\sigma > 0$ using, for instance, the parameterization in [Favaro et al. \(2013\)](#) (see their Section 3.1).

Summing up, both parameters have an effect on the number of clusters and the reinforcing mechanism. Interestingly, σ also enters the expression of the weights of existing clusters by reducing the probability of those with few elements. We refer to this double effect of σ as the “trade-off” between the number of clusters and reinforcement.

B.2 Linear generating model

In this simulation study we use a mechanism to generate the response that can be regarded as a specific case of the generating process presented in Section D.1. We do not apply any transformation to the data entering the continuation-ratio logistic function that takes predictive covariates as argument. In particular, right hand side of (D.1) reduces to $\alpha_k^a + \phi_k^a \psi(\mathbf{x}_i^a)$, and ϕ_k^a are set to $\phi^1 = (2.0, 2.6)^\top$, $\phi^2 = (-1.0, -3.0)^\top$. The simplification of the generative mechanism is evident because of the linearity in the relationship between the covariates and the probability of the outcome, as well as the specification of parameters to enforce a clear separation among treatments and categories.

The list of scenarios is designed as in the main simulation study.

Table A5 reports the results. The simpler generating mechanism results in overall better performances for all the methods, in particular we observe lower *MOT* and larger *%ΔMTU*. Unsurprisingly, dm-int demonstrates good performances, since it is the only model that assumes a (log-) linear relationship between covariates and outcome probabilities. Nonetheless, t-ppmx confirms to be a flexible and robust model, regardless of the generating mechanism. Among the two-stage methods, km-bp is the one that yields the better results.

	Scenario S1a			Scenario S1b		
	<i>MOT</i>	$\% \Delta MTU$	<i>NPC</i>	<i>MOT</i>	$\% \Delta MTU$	<i>NPC</i>
pam-bp	5.8200 (2.7899)	0.5995 (0.1691)	14.7400 (2.9124)	6.0200 (3.9096)	0.5439 (0.2626)	13.9400 (2.3248)
km-bp	4.3200 (2.6298)	0.6915 (0.1780)	14.9800 (2.6991)	5.0000 (2.7255)	0.6490 (0.1880)	12.9000 (2.4518)
hc-bp	6.6800 (1.7076)	0.5671 (0.1369)	14.5400 (2.7345)	6.5000 (2.0429)	0.5757 (0.1797)	12.4800 (1.8653)
dm-int	4.5400 (3.5869)	0.7258 (0.2219)	13.4800 (2.8084)	5.0800 (2.6484)	0.7027 (0.1635)	13.4600 (2.7346)
t-ppmx	4.4000 (2.5153)	0.7491 (0.1517)	14.8200 (2.4302)	5.5000 (3.0789)	0.6776 (0.2122)	14.4200 (2.7781)
	Scenario S2a			Scenario S2b		
	<i>MOT</i>	$\% \Delta MTU$	<i>NPC</i>	<i>MOT</i>	$\% \Delta MTU$	<i>NPC</i>
pam-bp	5.5600 (2.9358)	0.6112 (0.1847)	9.4400 (2.3488)	5.6800 (3.0199)	0.5693 (0.2012)	13.8400 (2.2710)
km-bp	4.2600 (2.8198)	0.7017 (0.1823)	10.7800 (2.1120)	5.0400 (2.3729)	0.6417 (0.1634)	13.0200 (2.3166)
hc-bp	7.0600 (2.1420)	0.5302 (0.1796)	11.6000 (2.6726)	6.7600 (1.7907)	0.5407 (0.1638)	12.5200 (1.9713)
dm-int	4.3600 (2.2656)	0.7376 (0.1354)	13.4000 (2.7180)	4.9800 (3.0937)	0.6962 (0.1994)	13.7400 (2.6171)
t-ppmx	5.0600 (2.5667)	0.7111 (0.1593)	14.9800 (2.6146)	5.1600 (3.0796)	0.6963 (0.2129)	14.9600 (2.5869)
	Scenario S3a			Scenario S3b		
	<i>MOT</i>	$\% \Delta MTU$	<i>NPC</i>	<i>MOT</i>	$\% \Delta MTU$	<i>NPC</i>
pam-bp	5.8600 (3.6868)	0.5983 (0.2398)	14.2000 (2.2406)	5.7400 (2.9194)	0.5597 (0.2059)	12.6400 (2.2475)
km-bp	4.9400 (3.6668)	0.6500 (0.2461)	14.6000 (2.2314)	4.9000 (3.3028)	0.6512 (0.304)	12.9200 (2.2932)
hc-bp	7.3400 (1.7798)	0.5167 (0.1473)	14.1000 (2.5414)	7.0000 (1.8844)	0.5289 (0.1761)	12.6800 (2.0247)
dm-int	3.5600 (2.2782)	0.7752 (0.1381)	13.9200 (3.1418)	4.5400 (2.1685)	0.7263 (0.1407)	13.7200 (2.4993)
t-ppmx	3.6000 (2.7180)	0.7913 (0.1603)	15.0600 (2.7435)	5.2600 (2.5380)	0.6956 (0.1521)	14.7400 (2.3974)

Table A5: Predictive performance: mean across 50 replicated datasets, standard deviations are in parentheses. In each scenario and for each index the best performance is in bold.

T-ppmx outperforms all competing models in terms of *NPC*. With respect to *MOT* and $\% \Delta MTU$, dm-int and t-ppmx present really close performances. Overall, t-ppmx attains better results when the number of covariates is moderate, while its predictive ability deteriorates as the number of predictive markers increase. Given that the two methods yield similar results, the great advantage provided by t-ppmx is that it allows for interpretable inference on the patients' clustering structure and identify patients more/less likely to benefit from a given treatment.

B.3 Recovering true clustering structure

We perform an additional comparative study to evaluate our method's ability to recover a latent structure in the data. We consider our predictive model with two different distributions for the random partition. In particular, we compare the proposed PPMx with a PPM employing the eppf induced by a DP as cohesion function. Note that such a PPM can be considered as a special case of our model, taking $\sigma = 0$ and $g(\mathbf{x}) \equiv 1$. Namely, we want to ascertain that the covariate-dependent prior we devised for the random partition adequately detects latent structure in the data.

We follow the generative mechanism described in Section 7.1, but instead of the data available from Golub et al. (1999), we use synthetic data –whose latent structure is known– as predictive biomarkers.

The first Scenario S1 closely follows [Argiento et al. \(2022\)](#). In particular, we generate 4 covariates (x_{i1}, \dots, x_{i4}) , for $i = 1, \dots, n$. The first two covariates are continuous, while the last two are binary. Covariates are independently generated from three groups, with sizes 75, 75, and 50, respectively, as follows:

$$(x_{i1}, x_{i2}) \stackrel{\text{iid}}{\sim} N_2(\boldsymbol{\mu}, 0.5I_2) \quad x_{i3}, x_{i4} \stackrel{\text{iid}}{\sim} \text{Bern}(q),$$

where I_2 is a 2×2 identity matrix. For the first group $\boldsymbol{\mu} = (-3, 3)^\top$ and $q = 0.1$. For the second one $\boldsymbol{\mu} = (0, 0)^\top$ and $q = 0.5$, while for the third one $\boldsymbol{\mu} = (3, 3)^\top$, $q = 0.9$.

Scenarios S2 and S3 follow the data generative mechanism 4 in [Page and Quintana \(2018\)](#). In particular, we consider Q covariates independently generated from the following distributions: 20% come from $N(0, 1)$, 20% from $U(0, 10)$, 20% from t_4 , (t distribution with 4 degrees of freedom), 20% more from $SN(10, 1, 10)$, (a skew-normal distribution) and the last 20% from a two-component mixture of the form $0.4N(0, 1) + 0.6N(10, 2)$. Scenarios S2 and S3 differ for the number of predictive covariates, that is, $Q = 10$ and $Q = 20$, respectively.

We use metrics presented in Section 7.2 to assess model prediction. We compute log pseudo-marginal likelihood (lpml) and Watanabe-Akaike Information Criterion (WAIC) to evaluate model fit. We generate 50 datasets for each scenario. Each generated dataset has $n = 200$ observations, with 170 classified as training observations.

Scenario S1						
	<i>MOT</i>	<i>%ΔMTU</i>	<i>NPC</i>	lpml	<i>ARI</i> ¹	<i>ARI</i> ²
PPM _x	9.9600 (4.3657)	0.4107 (0.2893)	16.6000 (2.6030)	-102.4659 (7.2650)	0.9491 (0.0380)	0.9608 (0.0578)
PPM	10.6800 (4.551)	0.3159 (0.3123)	15.5600 (2.4173)	-156.5070 (49.4241)	- -	- -
Scenario S2						
	<i>MOT</i>	<i>%ΔMTU</i>	<i>NPC</i>	lpml	<i>ARI</i> ¹	<i>ARI</i> ²
PPM _x	6.9200 (4.1837)	0.7387 (0.3581)	17.0000 (2.5395)	-101.4985 (30.3342)	0.5206 (5.1251)	0.4401 (0.1452)
PPM	11.0800 (6.7788)	0.3941 (0.5999)	15.7800 (2.8161)	-143.8411 (39.9999)	- -	- -
Scenario S3						
	<i>MOT</i>	<i>%ΔMTU</i>	<i>NPC</i>	lpml	<i>ARI</i> ¹	<i>ARI</i> ²
PPM _x	10.0200 (4.7915)	0.3742 (0.3592)	15.1800 (2.8190)	-104.5730 (6.5637)	0.5825 (0.0925)	0.5464 (0.1039)
PPM	10.8600 (6.4047)	0.2984 (0.4783)	15.2000 (2.6573)	-157.9971 (45.9023)	- -	- -

Table A6: Prediction performances, model fit measures, and ARI index for Treatment 1 and 2 for Scenarios S1-S3: mean across 50 replicated datasets (standard deviations are in parentheses).

We report averaged results in Table A6, with standard deviations in parenthesis. To evaluate our method's ability to recover a latent structure in the data, we also report ARI indices for PPM_x attained in the two treatments. PPM_x consistently outperforms PPM with respect to metrics evaluating prediction. PPM's poor performance is due to the response variable not being an explicit function of the covariates. Therefore, PPM can not recover any structure on the predictive covariates. For this reason, ARI is not computed for PPM.

B.4 Misspecification

A simulation study is conducted to assess the robustness of the method in the face of potential misspecification of prognostic and predictive covariates. To investigate the impact of missclassification on both clustering and predictive performance, two scenarios (S4 and S5) are constructed based on S2 and S3, where the clustering structure of the data is known. Specifically, building on Scenario S2, Scenario S4 was generated by designating two randomly selected predictive covariates as prognostic, and one of two randomly selected prognostic covariates as predictive. Similarly, Scenario S5 was created from Scenario S3 by randomly exchanging five of the 20 predictive covariates with one of the two prognostic covariates.

	<i>MOT</i>	$\% \Delta MTU$	<i>NPC</i>	lpml	<i>ARI</i> ¹	<i>ARI</i> ²
Scenario S4	10.4600 (5.4369)	0.4686 (0.4734)	15.0400 (2.6416)	-110.8869 (6.9667)	0.4015 (0.1713)	0.4159 (0.1573)
Scenario S5	11.7600 (4.5828)	0.2571 (0.3621)	12.9000 (3.1249)	-113.1016 (10.6491)	0.5682 (0.1849)	0.5705 (0.2023)

Table A7: Prediction performances, model fit measures, and ARI index for Treatment 1 and 2 for Scenarios S4-S5: mean across 50 replicated datasets (standard deviations are in parentheses).

T-ppmx shows to be quite robust to the misspecification of prognostic/predictive covariates. Specifically, when comparing the outcomes presented in Table A7 with those observed in Table A6 under scenarios S2 and S3, where no misspecification is present, it becomes evident that the t-ppmx approach is capable of recovering the clustering structure to a comparable extent. However, the results appear to be primarily impacted in terms of their predictive performance. In fact, the $\% \Delta MTU$ metric is considerably more affected by misspecification. Notably, the impact of misspecification is less severe in scenarios featuring a greater number of predictive covariates. This is exemplified by Scenario S5, which experiences a less significant loss with respect to Scenario S3, in contrast to the more pronounced effects seen comparing S4 to S2.

C Posterior Inference

We describe the MCMC algorithm to simulate from the posterior distribution of the parameters of interest:

$$\begin{aligned}
 p(\boldsymbol{\eta}^*, \mathcal{P}, \boldsymbol{\pi}, \boldsymbol{\beta} | \mathbf{y}, \mathbf{x}, \mathbf{z}) &= \prod_{a=1}^T p(\boldsymbol{\eta}^{a*}, \mathcal{P}_{n^a}^a, \boldsymbol{\pi}^a, \boldsymbol{\beta} | \mathbf{y}^a, \mathbf{x}^a, \mathbf{z}^a), \\
 p(\boldsymbol{\eta}^{a*}, \mathcal{P}_{n^a}^a, \boldsymbol{\pi}^a, \boldsymbol{\beta} | \mathbf{y}^a, \mathbf{x}^a, \mathbf{z}^a) &= \prod_{i=1}^{n_a} \pi_{iy_i^a}^{a*} \prod_{j=1}^{C_{n^a}^a} \prod_{i \in S_j^a} \text{Dirichlet}(\boldsymbol{\pi}_i^a | \boldsymbol{\gamma}_i^a(\boldsymbol{\eta}_j^{a*}, \boldsymbol{\beta})).
 \end{aligned} \tag{C.1}$$

We adopt a data augmentation approach (Argiento and De Iorio, 2022) to represent the Dirichlet distribution as independent latent Gamma random variables. In particular, we reparameterize equation 1 in the paper letting $\pi_{ik}^a = d_{ik}^a / D_i^a$, where $D_i^a = \sum_{k=1}^K d_{ik}^a$ and assume that $d_{ik}^a \sim \text{Gamma}(\gamma_{ik}^a(\boldsymbol{\eta}_{jk}^{a*}, \boldsymbol{\beta}_k), 1)$. More details in Section C.1.

The core part of the MCMC algorithm is the update of cluster membership. The computation associated with the joint law of $(\mathcal{P}_{n^a}^a, \boldsymbol{\eta}_j^{a*})$ is based on Neal (2000)’s Algorithm 8 with a reuse strategy (Favaro et al., 2013). Conditional on the updated cluster labels, all the remaining parameters are easily updated with Gibbs sampler or Metropolis-Hastings steps. In the following, we outline the implemented Metropolis-Hastings within Gibbs algorithm:

1. **update** $\{\mathcal{P}_{n^a}^a\}$ by Neal (2000)’s Algorithm 8 coupled with a reuse strategy Favaro et al. (2013);
2. **update** $\{\boldsymbol{\eta}_j^{a*}\}$ by Metropolis-Hastings. Hyperparameters are updated through Gibbs steps from their respective full conditional distributions;
3. **update** $\{(\kappa^a, \sigma^a)\}$ evaluating $p((\kappa^a, \sigma^a) | \mathcal{P}_{n^a}^a, \cdot)$ at a finite, discrete grid of possible (κ^a, σ^a) values;
4. **update** $\{\beta_{pk}\}$ by Metropolis-Hastings. Hyperparameters are updated through a slice sampler (Neal, 2003) as suggested in Polson et al. (2014);
5. **update** $\{d_{ik}^a\}$ drawing from its full conditional distributions, i.e. using Gibbs sampler.

A full discussion on the Metropolis within Gibbs we implemented is given in Section C.2. Finally in Section C.3 we discuss our approach for posterior clustering.

C.1 Augmented data scheme

Generating samples from the Dirichlet distribution using independent Gamma random variables is computationally efficient. Exploiting this property, we adopt a data augmentation approach based on a reparameterization of equation

1 in the paper and the introduction of an auxiliary parameter. We first assume that the response of the i -th patient to the treatment a follows a Multinomial distribution:

$$y_i^a | \pi_i^a \stackrel{\text{ind}}{\sim} \text{Multinomial}(1, \pi_i^a).$$

We assume a conjugate prior on the response probability

$$\pi_1^a, \dots, \pi_{n^a}^a | \eta_1^{a*}, \dots, \eta_{C_{n^a}^a}^{a*}, \mathcal{P}_{n^a}^a, \beta \sim \prod_{j=1}^{C_{n^a}^a} \prod_{i \in S_j^a} \text{Dirichlet}(\gamma_i^a(\eta_j^{a*}, \beta)).$$

We introduce latent random variables $d_{ik}^a \sim \text{Gamma}(\gamma_{ik}^a(\eta_{jk}^{a*}, \beta_k), 1)$ constructed such that $\pi_{ik}^a = d_{ik}^a / D_i^a$, where $D_i^a = \sum_{k=1}^K d_{ik}^a$, obtaining

$$y_i^a | \mathbf{d}_i^a, D_i^a \stackrel{\text{ind}}{\sim} \text{Multinomial}(1, \mathbf{d}_i^a / D_i^a),$$

where $\mathbf{d}_i^a = (d_{i1}^a, \dots, d_{iK}^a)^\top$.

Quantity $p(\eta^{a*}, \mathcal{P}_{n^a}^a, \pi^a, \beta | \mathbf{y}^a, \mathbf{x}^a, \mathbf{z}^a)$ in equation (C.1) can be restated as

$$p(\eta^{a*}, \mathcal{P}_{n^a}^a, \mathbf{d}^a, \beta | \mathbf{y}^a, \mathbf{x}^a, \mathbf{z}^a) = \prod_{i=1}^{n^a} \frac{d_{iy_i^a}^a}{D_i^a} \prod_{j=1}^{C_{n^a}^a} \prod_{i \in S_j^a} \text{Gamma}(\gamma_i^a(\eta_j^{a*}, \beta_k), 1), \quad (\text{C.2})$$

For $a = 1, \dots, T$, we introduce n^a auxiliary parameters u_i^a and let $u_i^a | D_i^a \sim \text{Gamma}(1, D_i^a)$. From the Gamma density function we obtain that

$$\frac{1}{D_i^a} = \int_0^\infty \exp(-D_i^a u_i^a) du_i^a,$$

so from equation (C.2):

$$\begin{aligned} p(\eta^{a*}, \mathcal{P}_{n^a}^a, \mathbf{d}^a, \beta, \mathbf{u} | \mathbf{y}^a, \mathbf{x}^a, \mathbf{z}^a) &= \prod_{i=1}^{n^a} d_{iy_i^a}^a e^{-D_i^a u_i^a} \left(\prod_{j=1}^{C_{n^a}^a} \prod_{i \in S_j^a} \prod_{k=1}^K \frac{d_{ik}^a \gamma_{ik}^a(\eta_{jk}^{a*}, \beta_k)^{-1} e^{-d_{ik}^a}}{\Gamma(\gamma_{ik}^a(\eta_{jk}^{a*}, \beta_k))} \right) \\ &= \prod_{i=1}^{n^a} d_{iy_i^a}^a e^{-u_i^a \sum_k d_{ik}^a} \left(\prod_{j=1}^{C_{n^a}^a} \prod_{i \in S_j^a} \prod_{k=1}^K \frac{d_{ik}^a \gamma_{ik}^a(\eta_{jk}^{a*}, \beta_k)^{-1} e^{-d_{ik}^a}}{\Gamma(\gamma_{ik}^a(\eta_{jk}^{a*}, \beta_k))} \right) \\ &= \prod_{i=1}^{n^a} d_{iy_i^a}^a \prod_{k=1}^K e^{-u_i^a d_{ik}^a} \left(\prod_{j=1}^{C_{n^a}^a} \prod_{i \in S_j^a} \prod_{k=1}^K \frac{d_{ik}^a \gamma_{ik}^a(\eta_{jk}^{a*}, \beta_k)^{-1} e^{-d_{ik}^a}}{\Gamma(\gamma_{ik}^a(\eta_{jk}^{a*}, \beta_k))} \right) \\ &= \prod_{i=1}^{n^a} d_{iy_i^a}^a \left(\prod_{j=1}^{C_{n^a}^a} \prod_{i \in S_j^a} \prod_{k=1}^K \frac{d_{ik}^a \gamma_{ik}^a(\eta_{jk}^{a*}, \beta_k)^{-1} e^{-d_{ik}^a (u_i^a + 1)}}{\Gamma(\gamma_{ik}^a(\eta_{jk}^{a*}, \beta_k))} \right). \end{aligned}$$

C.2 MCMC sampling

For the posterior inference, we designed a Metropolis within Gibbs sampler. We use Algorithm 8 by Neal (2000) with a reuse strategy (Favaro et al., 2013) for cluster label updates.

We introduce here the latent cluster allocations. In particular, for $a = 1, \dots, T$, let $e^a = (e_1^a, \dots, e_{n^a}^a)^\top$ be the cluster allocation vector of indexes, with $e_i^a = j$ iff $i \in S_j^a$. Conditional on the updated cluster labels, all the remaining parameters are updated with Gibbs sampler or Metropolis-Hastings steps. We briefly outline the scheme in Algorithm 1, and we give full details in the following.

$\mathcal{P}_{n^a}^a$: *Algorithm 8 with Reuse.* For $a = 1, \dots, T$, and $i = 1, \dots, n^a$, let $S_j^{a,-i}$ and $C_{n^a}^{a,-i}$ denote the j -th cluster and the total number of clusters when subject i assigned to treatment a is not considered. In the same way, we use $\mathbf{x}_j^{a*, -i}$ to denote the matrix of predictive determinants of the patients in cluster j when the i -th patient is not

Algorithm 1: MCMC sampling

```

1 for  $l = 1, \dots, niter$  do
2   for  $a = 1, \dots, T$  do
3     /* Algorithm 8 with Reuse */
4     Update the random partition  $\mathcal{P}_{n^a}$ 
5     for  $a = j, \dots, C_{n^a}^a$  do
6       /* Metropolis step */
7       Update the cluster specific parameters  $\eta_j^{a*}$ 
8       /* Gibbs step */
9       Update the hyperparameters of the cluster specific parameters  $(\theta^a, \Lambda^a)$ 
10      /* Gibbs step */
11      Update the NGGP parameters  $(\kappa^a, \sigma^a)$ 
12    /* Metropolis step */
13    Update prognostic coefficients  $\{\beta_{pk}\}_{p=1, \dots, P, k=1, \dots, K}$ 
14    /* Slice sampler */
15    Update hyperparameters of the prognostic coefficients  $\{\lambda_{pk}\}_{p=1, \dots, P, k=1, \dots, K}$  and  $\{\tau_k\}_{k=1, \dots, K}$ 
16    for  $a = 1, \dots, T$  do
17      /* Gibbs step */
18      Update latent random variable  $\{d_{ik}^a\}_{i=1, \dots, n^a, k=1, \dots, K}$ 
19      /* Gibbs step */
20      Update auxiliary parameters  $\{u_i^a\}_{i=1, \dots, n^a}$ 
    
```

included. Cluster membership for patient i that is e_i^a is drawn using the following unnormalized probabilities:

$$P(e_i^a = j | \cdot) \propto \begin{cases} \prod_{k=1}^K \frac{d_{ik}^a \gamma_{ik}^a (\eta_{jk}^{a*}, \beta_k)^{-1} e^{-d_{ik}^a (u_i^a + 1)}}{\Gamma(\gamma_{ik}^a (\eta_{jk}^{a*}, \beta_k))} \frac{\rho(S_j^{a,-i} \cup \{i\}) g(\mathbf{x}_j^{a*,-i} \cup \{\mathbf{x}_i^a\})}{\rho(S_j^{a,-i}) g(\mathbf{x}_j^{a*,-i})} & \text{for } j = 1, \dots, C_{n^a}^{a,-i} \\ \prod_{k=1}^K \frac{d_{ik}^a \gamma_{ik}^a (\eta_{jk}^{a*}, \beta_k)^{-1} e^{-d_{ik}^a (u_i^a + 1)}}{\Gamma(\gamma_{ik}^a (\eta_{jk}^{a*}, \beta_k))} \frac{\rho(\{i\}) g(\{\mathbf{x}_i^a\})}{M} & \text{for } j = C_{n^a}^{a,-i} + 1, \dots, C_{n^a}^{a,-i} + M, \end{cases} \quad (C.3)$$

where $\{\eta_{jk}^{a*}\}$ for $j = C_{n^a}^{a,-i} + 1, \dots, C_{n^a}^{a,-i} + M$ are M auxiliary variables (Neal, 2000), associated with M empty clusters, independently and identically distributed according to some prior distribution p^e . The first terms are the likelihoods associated with observation i given the clusters' parameters. The second terms can be interpreted as being proportional to the covariate-informed prior probability of being assigned to the corresponding cluster (with the M empty clusters sharing the probability of creating a new cluster).

Algorithm 8 with Reuse proposes efficient handling of the M auxiliary parameters; it updates the cluster assignment of observation i according to the following scheme reported in Algorithm 2.

In the original formulation of Algorithm 8 (Neal, 2000), after the update of the cluster label, the auxiliary parameters associated with empty clusters are discarded. Since after the cluster update for the i -th subject, the parameters for unused empty clusters are already independently and identically distributed, Favaro et al. (2013) propose to reuse them for the update of the subsequent observations. Note that the only difference adopting the Reuse Algorithm implies is the way the parameters of the empty clusters are managed and retained across cluster assignment updates of multiple observations.

Finally, particular attention should be paid to the relabeling step at line 6 of Algorithm 2. In fact, to avoid gaps in the cluster labels we need to relabel all the clusters (Page and Quintana, 2015). We denote with $\mathbf{e}^{a,-i} = (e_1^a, \dots, e_{n^a-1}^a)^\top$ the cluster allocation vector of indices when subject i assigned to treatment a is not considered. We relabel $\{S_{j'}^{a,-i} : S_{j'}^{a,-i} > S_j^a\}$ for $j' = 1, \dots, C_{n^a}^{a,-i}$. In particular, if $S_{j'}^{a,-i} > S_j^a$, $S_{j'}^{a,-i} = S_{j'}^{a,-i} - 1$, for $j' = 1, \dots, C_{n^a}^{a,-i}$. Similarly, we relabel $\{e_{i'}^{a,-i} : e_{i'}^{a,-i} > e_i^a\}$ for $i' = 1, \dots, n^a - 1$. In particular, if $e_{i'}^{a,-i} > e_i^a$, $e_{i'}^{a,-i} = e_{i'}^{a,-i} - 1$, for $i' = 1, \dots, n^a - 1$.

η_j^{a*} : *Metropolis step.* For $a = 1, \dots, T$, $j = 1, \dots, C_{n^a}^a$ we propose η_j^{a*} obtained from a random walk proposal and accept it with probability

Algorithm 2: Algorithm 8 with Reuse

```

1 for  $a = 1, \dots, T$  do
2   for  $i = 1, \dots, n^a$  do
3     Remove  $i$  from the cluster it belongs, so that  $S_j^a \in \mathcal{P}_n^a, |S_j^a| = n_j^a$  becomes  $S_j^{a,-i}, |S_j^{a,-i}| = n_j^a - 1$ 
4     if  $|S_j^a| = 0$  /* Cluster  $S_j^a$  is empty */
5       then
6         Relabel  $S^{a,-i}$  and  $e^{a,-i}$  to avoid gaps in the cluster labels
7         Sample  $m \in \{1, \dots, M\}$  uniformly at random
8         Replace  $\eta_{C_{n^a}^{a,-i}+m}^{a*}$  with  $\eta_j^{a*}$ 
9         Remove  $S_j^a$  from  $\mathcal{P}_{n^a}^a$ 
10    Assign  $i$  to the clusters with probabilities  $P(e_i^a = j \mid \cdot)$ 
11    if  $e_i^a \in \{C_{n^a}^{a,-i} + 1, \dots, C_{n^a}^{a,-i} + M\}$ 
12      /* The observation  $i$  is assigned to an empty cluster */
13      then
14        Assign it to a new cluster in  $\mathcal{P}_n^a$  with parameter  $\eta_{e_i^a}^{a*}$ 
15        Replace  $\eta_{e_i^a}^{a*}$  with a new independent draw from  $p^e$ .
16  /* Now we update empty clusters' parameters with the Reuse strategy */
17  Discard  $\{\eta_j^{a*}\}$  for  $j = C_{n^a}^a + 1, \dots, C_{n^a}^a + M$ 
18  Sample  $M$  iid  $\{\eta_j^{a*}\}$ s from  $p^e$  (for  $j = C_{n^a}^a + 1, \dots, C_{n^a}^a + M$ )
    
```

$$\min \left\{ \frac{p(\mathbf{d}^a \mid \eta_j^{a*}, \cdot) p(\eta_j^{a*})}{p(\mathbf{d}^a \mid \eta_j^{a*}, \cdot) p(\eta_j^{a*})}, 1 \right\}.$$

Hyperparameters update:

θ^a, Λ^a *Gibbs step.* For $a = 1, \dots, T$ we sample θ^a and Λ^a from their respective full conditionals:

$$\theta^a \mid \Lambda^a, \eta_1^{a*}, \dots, \eta_j^{a*} \sim N_K \left(\frac{\mu_0 \nu_0 + n^a}{n^a + \nu_0}, (\Lambda^a (n^a + \nu_0))^{-1} \right),$$

$$\Lambda^a \mid \eta_1^{a*}, \dots, \eta_j^{a*} \sim W \left(s_0 + \frac{n^a}{2}, \Lambda_0 + \frac{n^a}{2} (\bar{\Lambda}^a + \frac{s_0}{s_0 + n^a} (\bar{\eta}^a - \mu_0)(\bar{\eta}^a - \mu_0)^\top) \right),$$

$$\text{where } \bar{\eta} = (\bar{\eta}_1, \dots, \bar{\eta}_K)^\top, \bar{\eta}_k = \frac{1}{n} \sum_{j=1}^{C_{n^a}^a} \eta_{jk}^{a*} n_j, \text{ and } \bar{\Lambda} = \frac{1}{n} \sum_{i=1}^n (\eta_i - \bar{\eta})(\eta_i - \bar{\eta})^\top.$$

(κ^a, σ^a) : *Gibbs step.* Since the normalizing constant of equation (4.3) can not be computed, we produce samples from a discretized approximation of posterior distribution, evaluating $p((\kappa^a, \sigma^a) \mid \mathcal{P}_n^a, \cdot)$ at a finite, discrete grid of possible (κ^a, σ^a) values. In particular, we construct a 10×10 grid in $(0, 15) \times (0.0, 0.6)$, such that the marginal distributions are $\kappa \sim \text{Gamma}(2, 1)$ and $\sigma \sim \text{Beta}(5, 23)$, respectively. For $a = 1, \dots, T$, we evaluate (4.3) at each grid point, obtaining a discrete approximation of the log posterior distribution, and then we normalize the values, obtaining weights that sum to 1 across the grid's points. Finally, we sample a new value for (κ^a, σ^a) from the grid with respect to their corresponding normalized posterior probability.

β_{pk} : *Metropolis step.* For $k = 1, \dots, K$, we propose β_{pk} from a random walk proposal and accept it with probability:

$$\min \left\{ \frac{p(\mathbf{d}^a \mid \beta_{pk}', \cdot) p(\beta_{pk}')}{p(\mathbf{d}^a \mid \beta_{pk}, \cdot) p(\beta_{pk})}, 1 \right\}.$$

Hyperparameters update:

λ_{pk} The global scale parameters are updated through an adaptation of the slice sampling scheme given in the online supplement of Polson et al. (2014). For $p = 1, \dots, P$ and $k = 1, \dots, K$, we define $\varpi_{pk} = 1/\lambda_{pk}^2$

and $\varsigma_{pk} = \beta_{pk}/\tau_k$. This reparameterization allows us to employ slice sampler (Neal, 2003), as the conditional posterior distribution of ϖ_{pk} is

$$p(\varpi_{pk} \mid \tau_k, \varsigma_{pk}) \propto \exp \left\{ -\frac{\varsigma_{pk}^2}{2} \varpi_{pk} \right\} \frac{1}{1 + \varpi_{pk}}.$$

To sample λ_{pk} :

1. draw a sample from Uniform distribution:

$$h_{pk} \mid \varpi_{pk} \sim U(0, 1/(1 + \varpi_{pk}));$$

2. draw a sample from Truncated Exponential density, so that it has zero probability outside the interval $(0, (1 - u_{pk})/u_{pk})$:

$$\varpi_{pk} \mid \varsigma_{pk}, h_{pk} \sim \text{Exp}(2/\varsigma_{pk}^2).$$

Transforming back to the λ -scale it will ensure a sample from the conditional distribution of interest.

τ_k The same applies for τ_k , replacing $\varpi = 1/\tau_k^2$ and $\varsigma_k^2 = \sum_{p=1}^P \beta_{pk}^2/2$, for $k = 1, \dots, K$.

d_{ik}^a : *Gibbs step.* For $a = 1, \dots, T, i = 1, \dots, n^a$ and $k = 1, \dots, K$ we sample d_{ik}^a from:

$$d_{ik}^a \mid \cdot \sim \text{Gamma}(\gamma_{ik}^a(\eta_{jk}^{a*}, \beta_k) + \delta_1(y_i^a), (u_i^a + 1)^{-1}).$$

where δ_1 is a $K \times 1$ vector of zeros, with y_i^a -th element equal to 1.

u_i^a : *Gibbs step.* For $a = 1, \dots, T, i = 1, \dots, n^a$ we sample u_i^a from:

$$u_i^a \mid \cdot \sim \text{Gamma}(1, D_i^{a-1}).$$

C.3 Posterior Clustering

The main inferential goal of our method is treatment prediction. The covariate-dependent random partition model is employed to obtain homogeneous groups of patients. Posterior inference for the random partition $\mathcal{P}_{n^a}^a$ is affected by label switching. Since symmetric priors are chosen for both the random partition $\mathcal{P}_{n^a}^a$ and cluster-specific parameters $p^*(\zeta^{a*})$, their posterior distribution is invariant under permutations of the component indices. As a consequence, cluster labels are not identifiable. Nonetheless, prediction is not affected by label-switching because the posterior predictive distribution marginalizes over all possible partitions (Müller et al., 2011). Let \tilde{x} and \tilde{z} denote predictive and prognostic markers of a new patient. Following Müller et al. (2011), we predict the response of the new untreated patient through an importance sampling strategy as follows: at each step of the MCMC algorithm, given the current partition we first assign a new patient to a cluster using the following probability weights

$$w_j^a \propto \begin{cases} \frac{\rho(S_j^a \cup \{n^a + 1\})g(\mathbf{x}_j^{a*} \cup \{\tilde{x}^a\})}{\rho(S_j^a)g(\mathbf{x}_j^{a*})} & \text{for } j = 1, \dots, C_{n^a}^a \\ \rho(\{n^a + 1\})g(\{\tilde{x}^a\}) & \text{for } j = C_{n^a}^a + 1, \dots, C_{n^a}^a + M \end{cases} \quad (\text{C.4})$$

and then we generate the cluster-specific parameters $\hat{\eta}_j$ weighted by w_j 's. Given these parameter values, we can predict the response probabilities of the new patient simply by applying the multinomial response model; see also Page and Quintana (2016) for a similar approach.

Finally, the marginal posterior distribution for the number of clusters $p(C_{n^a}^a \mid y_1^a, \dots, y_{n^a}^a, \mathbf{x}_1^a, \dots, \mathbf{x}_Q^a)$ is available as a byproduct of the posterior distribution for the random partition. To obtain a point estimate for $p(\mathcal{P}_{n^a}^a \mid y_1^a, \dots, y_{n^a}^a, \mathbf{x}_1^a, \dots, \mathbf{x}_Q^a)$ we follow Wade and Ghahramani (2018) and adopt a decision-theoretic approach that uses the variation of information loss function on the space of clusterings to estimate the optimal partition and to characterize its uncertainty.

D Generating Mechanism

We closely follow the strategy devised in Ma et al. (2016, 2019) to generate the simulated datasets, i.e., we do not employ our model as the generative mechanism. To emulate the complex correlation patterns of genomics data, we obtain prognostic and predictive covariates from a leukemia dataset. The data available from Golub et al. (1999) provide gene expression levels from 5000 genes collected across 38 patients, of which 11 were diagnosed with acute myelogenous leukemia and the remaining with acute lymphoblastic leukemia. To obtain scenarios with larger sample size, Ma et al. (2016, 2019) devised a procedure to expand the dataset, yielding $n = 152$ patients (38×4) with

Algorithm 3: Posterior Predictive sampling

```

1 for  $a = 1, \dots, T$  do
2   Compute  $g(\tilde{\mathbf{x}}^{a*})$ 
3   for  $j = 1, \dots, C_{n^a}$  do
4     Compute  $g(\mathbf{x}_j^{a*})$ 
5   for  $j = C_{n^a} + 1, \dots, C_{n^a} + M$  do
6     Compute  $g(\mathbf{x}_j^{a*} \cup \{\tilde{\mathbf{x}}^a\})$ 
7   for  $j = 1, \dots, C_{n^a} + M$  do
8     Compute  $w_j$  from equation (C.4)
9   Sample  $e_i^a$  from  $Multinomial(\mathbf{w}^a)$ 
10  if  $e_i^a \in \{C_{n^a} + 1, \dots, C_{n^a} + M\}$ 
11    /* The observation  $\tilde{i}$  is assigned to an empty cluster */
12    then
13      Assign it to a new cluster in  $\mathcal{P}_{n^a}^a$  with parameter  $\eta_{e_i^a}^{a*}$  obtained from a new independent draw from  $G_0$ 
14    Compute  $\{\log(\gamma_{ik}^a(\eta_{e_i^a}^{a*}, \beta_k))\}_{k=1, \dots, K}$  from equation (2) in the main paper
15    Draw  $\pi_i^a$  from equation (1) in the main paper
16    for  $k = 1, \dots, K$  do
17      Sample  $\tilde{y}$  from  $p(\tilde{y}^a = k \mid \mathbf{y}^a, \mathbf{z}^a, \mathbf{x}^a, \tilde{\mathbf{z}}, \tilde{\mathbf{x}})$ 
    
```

$Q = 90$ predictive and $P = 2$ prognostic biomarkers. This data-processing procedure is presented in detail in the Supplementary material of Ma et al. (2019). The patients are assigned to $T = 2$ competing treatment, and $K = 3$ levels of the ordinal-valued response variable are considered. Since the observed treatment endpoints were unavailable, the treatment response is generated using two continuation-ratio logistic functions (see Supplementary Material for more details). Finally, the optimal treatment for each simulated patient is determined as the inner product between the ordinal response probability and the response level utility weight ω . In particular, we set $\omega = (0, 40, 100)^\top$ to make the ordinal response reflect the clinical importance of each level (Ma et al., 2016).

D.1 Generating treatment response

The data available from Golub et al. (1999) do not provide the observed treatment endpoints, so the treatment response is generated using two continuation-ratio logistic functions.

The first one takes predictive biomarkers as arguments:

$$r_k(\mathbf{x}_i^a) = \log \left(\frac{Pr(y_i^a = k \mid \mathbf{x}_i^a)}{p(y_i^a < k \mid \mathbf{x}_i^a)} \right) = \alpha_k^a + \phi_k^a \psi(\mathbf{x}_i^a)^3, \text{ for } i = 1, \dots, n^a, \quad (\text{D.1})$$

where $\psi(\cdot)$ is a one-dimensional function of the first two principal components, used to summarize the information carried by predictive markers. Response-level probabilities for prognostic features are defined through the second continuation-ratio logistic function:

$$r_k^*(\mathbf{z}_i^a) = \log \left(\frac{Pr(y_i^a = k \mid \mathbf{z}_i^a)}{p(y_i^a < k \mid \mathbf{z}_i^a)} \right) = \iota_k + \chi_k \mathbf{z}_i^a, \text{ for } i = 1, \dots, n^a. \quad (\text{D.2})$$

The coefficients α_k^a , ϕ_k^a , ι_k^a and χ_k , for $k = 1, \dots, K - 1$, are set to value that could produce realistic response rates. In particular, $\alpha^1 = (-0.5, -1.0)^\top$, $\alpha^2 = (0.7, -1.0)^\top$, $\phi^1 = (1.5, 2.0)^\top$, $\phi^2 = (-0.5, -1.0)^\top$, $\iota = (1.0, -0.5)^\top$, $\chi^1 = (1.0, 0.5)^\top$, and $\chi^2 = (0.7, 1.0)^\top$. The probabilities for each level of the ordinal response variable were generated as the pointwise product of (D.1) and (D.2) for each patient. That is, the true ordinal response probability (ORP) for response k

$$ORP_{ik}^a = \frac{\omega_k (r_k(\mathbf{x}_i^a) r_k^*(\mathbf{z}_i^a))}{\sum_{k=1}^K \omega_k (r_k(\mathbf{x}_i^a) r_k^*(\mathbf{z}_i^a))}, \quad i = 1, \dots, n^a.$$

See Ma et al. (2019) for more details.

E Additional details of performance metrics

E.1 Construction of $\% \Delta MTU$ index

The extent to which a treatment is beneficial for each patient is heterogeneous, and the improvement offered by a therapy varies from patient to patient. In order to account for this heterogeneity, performances should be evaluated considering the relative utility gain. The relative gain in Treatment Utility, $\% \Delta MTU$ (Ma et al., 2016) allows measuring the overall benefit ensured by a treatment selection rule in the case of $T = 2$ competing treatments. Denoting with $MTU^a(i)$ the mean treatment utility of treatment a for patient i , we can obtain the differential treatment utility as $\Delta MTU(i) = MTU^1(i) - MTU^2(i)$. Considering the true optimal treatment $A(i)$ and denoting with $t(i)$ the treatment recommended by selection rule, we can construct the indicator function $\delta_{t(i)}(A(i))$ that is defined as:

$$\delta_{t(i)}(A(i)) = \begin{cases} 1 & \text{if } t(i) = A(i) \\ -1 & \text{if } t(i) \neq A(i). \end{cases}$$

The sum of the true gains achieved by the selection rule is

$$\Delta MTU = \sum_{i=1}^n \delta_{t(i)}(A(i)) |\Delta MTU(i)|.$$

The maximum possible gain in mean treatment utility varies in each simulation scenario. To make performance comparable also across scenarios, we consider the proportion of the maximum possible gain in total mean treatment utility attained by the selection rule, that is:

$$\% \Delta MTU = \Delta MTU / \Delta MTU_{opt},$$

where ΔMTU_{opt} is the maximum possible total MTU , achieved when all patients are assigned to their optimal treatment. Finally, $\% \Delta MTU$ is bounded above by 1 when it always recommends the optimal treatment, and $\% \Delta MTU = -1$ when it fails to select the optimal therapy for all the patients.

E.2 Empirical Summary Measure (ESM)

TCGA data do not provide the true optimal treatment, and only the NPC measure, among those discussed in Section 6.1, can be used. We employ an empirical summary measure (ESM, Song and Pepe, 2004) to evaluate the relative increase in the population response rate attributable to a treatment allocation method compared to random allocation. Let Y be the binary outcome variables, taking 0 for non-respondents or 1 for respondent patients. We define the treatment contrast as $\Delta(\mathbf{X}, \mathbf{Z}) = Pr(Y = 1 | A = 2, \mathbf{X}, \mathbf{Z}) - Pr(Y = 1 | A = 1, \mathbf{X}, \mathbf{Z})$, where $A = \{1, 2\}$ denote the non-targeted and targeted treatment, respectively. Indicating with $Pr(Y = 1 | A_r)$ the probability of being a respondent under a randomized treatment assignment, we obtain the relative increase in the population response rate under a personalized treatment selection rule as:

$$ESM = \{Pr(Y = 1 | A = 2, \Delta(\mathbf{X}, \mathbf{Z}) > 0) \times Pr(\Delta(\mathbf{X}, \mathbf{Z}) > 0) + \\ Pr(Y = 1 | A = 1, \Delta(\mathbf{X}, \mathbf{Z}) < 0) \times Pr(\Delta(\mathbf{X}, \mathbf{Z}) < 0)\} - Pr(Y = 1 | A_r),$$

where $Pr(Y = 1 | A = 2, \Delta(\mathbf{X}, \mathbf{Z}) > 0)$ and $Pr(Y = 1 | A = 1, \Delta(\mathbf{X}, \mathbf{Z}) < 0)$ can be estimated as the response rates for the subset of patients assigned by the proposed method to the treatment actually received; $Pr(\Delta(\mathbf{X}, \mathbf{Z}) > 0)$ and $Pr(\Delta(\mathbf{X}, \mathbf{Z}) < 0)$ can be empirically estimated as the proportion of patients who are recommended for targeted and standard treatment, respectively. Let n^1 and n^2 be the number of patients that received treatment $A = 1$ and $A = 2$, respectively; the weights $Pr(\Delta(\mathbf{X}, \mathbf{Z}) > 0)$ and $Pr(\Delta(\mathbf{X}, \mathbf{Z}) < 0)$ can be estimated as n^1/n and n^2/n , respectively. Finally, $Pr(Y = 1 | A_r)$ is the overall response rate under randomization, and can be estimated as the sample proportion of responders.

Note that we based this summary measure on only two response categories, responders (CR) and non-responders (PD + PS), whereas we used all three levels of the ordinal outcome in the data analysis and to implement personalized treatment selection.

F Data pre-processing in Ma et al. (2019)

In our study, we analyzed data from Ma et al. (2019). As the TCGA data used in the study were collected from observational studies, measures were taken to avoid potential bias by matching patients based on baseline covariates

such as tumor grade, gender, age, and initial year of pathological diagnosis (IYPD). To achieve this, they used the R package *MatchIt* (Stuart et al., 2011) with default settings, resulting in 79 pairs of patients with standardized mean differences of 0.000, -0.050, 0.051, and 0.162 for tumor grade, gender, age, and IYPD, respectively. Obtained matches were reasonably satisfactory, as all final standardized mean differences were below the suggested cut-off value of 0.25 (Imai et al., 2008). Moreover, in Ma et al. (2019), to identify potential prognostic and predictive features among the 173 protein expressions measured in the LGG dataset, univariate logistic regression models were fitted with a protein, the treatment, and their interaction as covariates using the MASS package in R (Ripley et al., 2013). A protein was considered as predictive (prognostic) if the P -value obtained from Wald’s test for the interaction (main) effect was less than 0.1. Using this criterion, 23 proteins were selected as potential predictive features and five as potential prognostic features. The complete list of predictive proteins is reported in Table A8.

ACVRL1	Src	HSP70	HER2	PAI-1	Smad
FOXO3a	PRAS40	Cyclin	SF2	Bad	Lck
Caspase-7-cleavedD198	Paxillin	MYH11	$14 - 3 - 3 - \epsilon$	Akt	Caveolin-1
Rab25	YAP	RBM15	Claudin-7	ER- α	C-Raf
CD31	Ku80	Bcl-2	GSK3- α - β		

Table A8: List of predictive proteins used in the LGG case study.

In the subsequent analysis, two prognostic covariates, namely ACVRL1-R-C and HSP70-R-C, were utilized as they exhibited the highest accuracy rate (78/158) in discriminant analysis. This analysis was conducted using 79 pairs of matched data with binary outcomes of PD/SD/PR as 0 and CR as 1.

G MCMC Diagnostic Checks for LGG Data Analysis

Convergence has been assessed through Gelman-Rubin potential scale reduction factor (PSRF, Gelman and Rubin, 1992) for parameters associated with prognostic covariates.

1.0909	1.0173	1.1129
1.1159	1.1102	1.0991

Table A9: Potential Scale Reduction Factor for prognostic covariates’ regression coefficients $\{\beta_{pk}\}$.

To assess the goodness-of-fit and the convergence of the parameters involved in the PPMx, we report in Figures 5 and 6 the trace plots of the number of clusters and the $lpml$, respectively. In both cases, the trace plots are displayed separately for each fold.

These results do not raise any particular concerns on the MCMC convergence.

H Additional Figure

Our PPMx model provides homogeneous clusters in terms of predictive covariates so that the resulting clustering represents a compact data partitioning. It substantially reduces the within-group variance for each predictive covariate, as displayed in Figure 7. Predictive covariates are standardized, so it is clear that there is a dramatic reduction in within-group variance for most of the predictive biomarkers. Some proteins still show a pronounced variance. Since it happens mainly in T1G6, T2G5, and T2G10, it is likely due to the small number of patients clustered together in these groups (2, 2, and 3 patients, respectively).

I Additional Simulations for LGG data

In order to assess the robustness of the results for LGG data analysis, we run additional analysis. The results of the simulation study are reported in Table A10. Since the number of correctly predicted outcome (NPC) does not depend on the weights, we report here only the Empirical Summary Measure (ESM).

We find that the method is robust to different elicitation of ω_2 , and that the results are consistent with those reported in the paper.

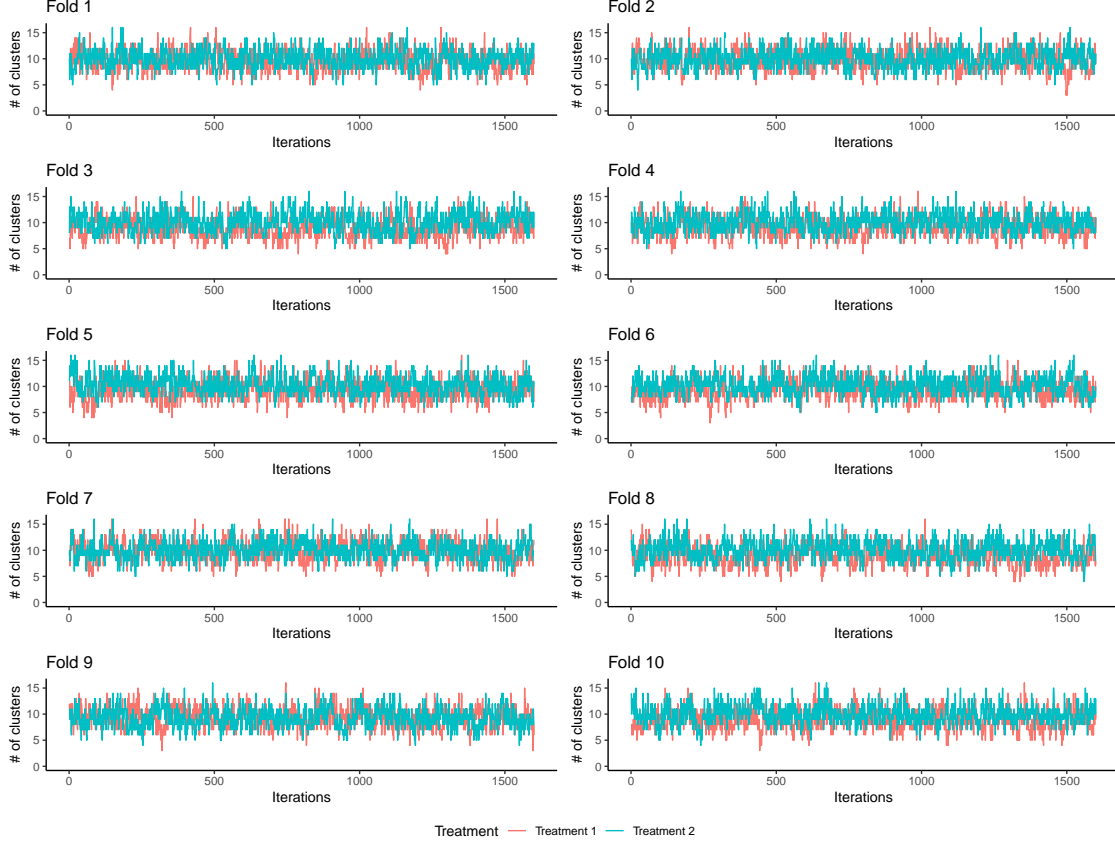


Figure 5: Traceplots of the number of clusters.

ω_2	20	40	60	80
pam-bp	0.0701	0.0553	0.0401	0.0388
km-bp	0.0295	0.0384	0.0335	0.0199
hc-bp	0.0770	0.0285	0.0170	0.0185
dm-int	0.0746	0.0746	0.0970	0.0876
t-ppmx	0.1015	0.1008	0.1020	0.0751

Table A10: Results of 10-fold cross-validation to obtain the ESM for different values of the weight for the partial response, ω_2 . The weights for Progressive Disease and Complete Response are fixed at $\omega_1 = 0$ and $\omega_3 = 100$, respectively. The best performance for each ω_2 value is highlighted in bold.

To evaluate the impact of combining PR and SD, we performed an analysis of LGG data considering the four RECIST categories for the response. The results of this analysis are presented in Table A11. We evaluate the number of correctly predicted outcome (NPC) and the Empirical Summary Measure (ESM). Note that ESM is based on only two response categories, responders (CR) and non-responders (PD + PR + SD), whereas we used all four levels of the ordinal outcome in the data analysis and to implement personalized treatment selection.

Compared to the results obtained using three categories for the outcome, we observed a general improvement for all methods in terms of ESM. While the two-step methods proposed by Ma et al. (2019) showed a slight improvement in NPC, dm-int and t-ppmx exhibited a deterioration. However, this additional evaluation confirmed that our method outperforms all competitors in treatment selection.

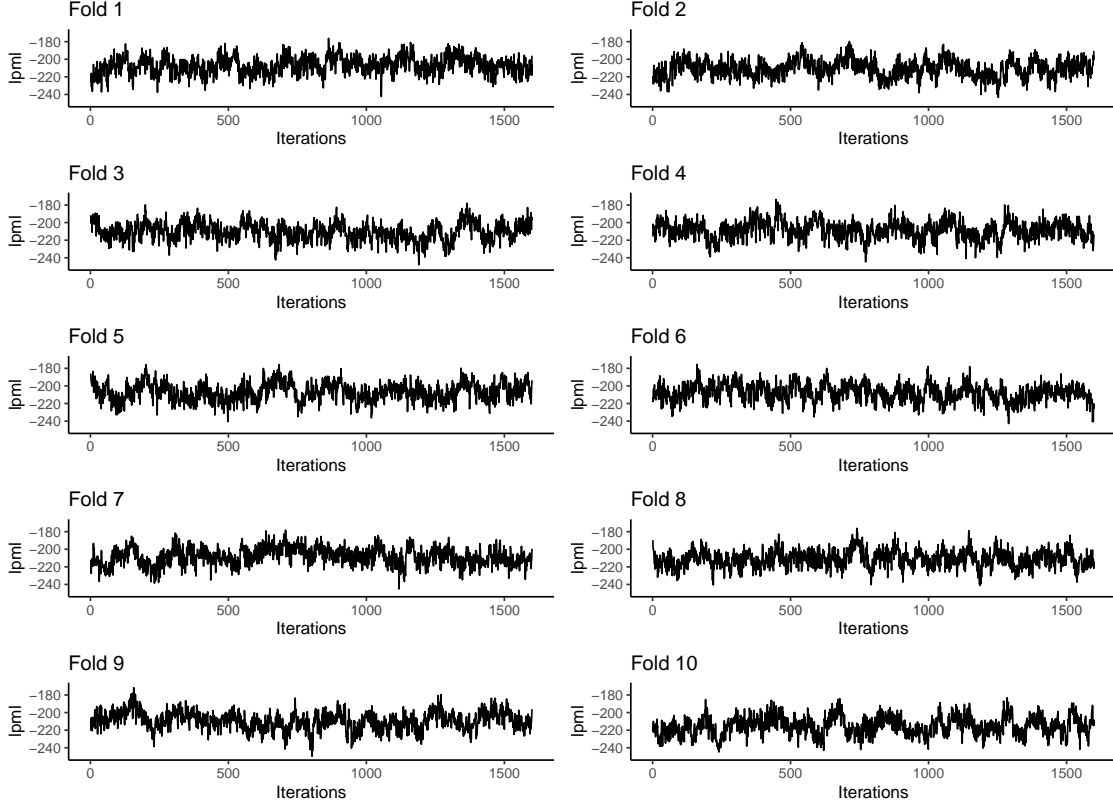


Figure 6: Traceplots of the lpml.

	NPC	$ESM (> 3)$
pam-bp	51	0.0809
km-bp	53	0.0134
hc-bp	53	0.0582
dm-int	54	0.0840
t-ppmx	50	0.1259

Table A11: Predictive performance with four RECIST categories: metrics were obtained using 10-fold cross-validation. To compute ESM, the fourth RECIST category (Complete Response) was considered as the response. The best performance for each index is highlighted in bold.

J Alternative Likelihoods

We would like to acknowledge that beyond the Dirichlet-multinomial likelihood, there are alternative functions worth considering. For instance, the multinomial logit model presents a viable option that might yield comparable predictive performance. However, it is important to note that interpreting the multinomial logit parameters can be less straightforward since they represent log odds ratios with respect to a specific baseline response level. Furthermore, given the ordinal nature of our response variable, ordinal regression emerges as a compelling and valid choice. This model allows us to effectively accommodate the ordered categories while maintaining the interpretability of results in terms of the ordinal relationship between response levels. Notably, in a study by [Page et al. \(2021\)](#), an ordinal response for a PPMx model has been considered by assuming it to be a discretization of a continuous, real-valued latent score. To achieve this, fixed thresholds were introduced to create the ordinal categories. However, we recognize that this strategy has inherent limitations, as the outcomes may be sensitive to the choice of cutoff values. To address this concern, a potential solution could involve estimating the latent cutoffs as unknown parameters, which could lead to more robust and reliable results.

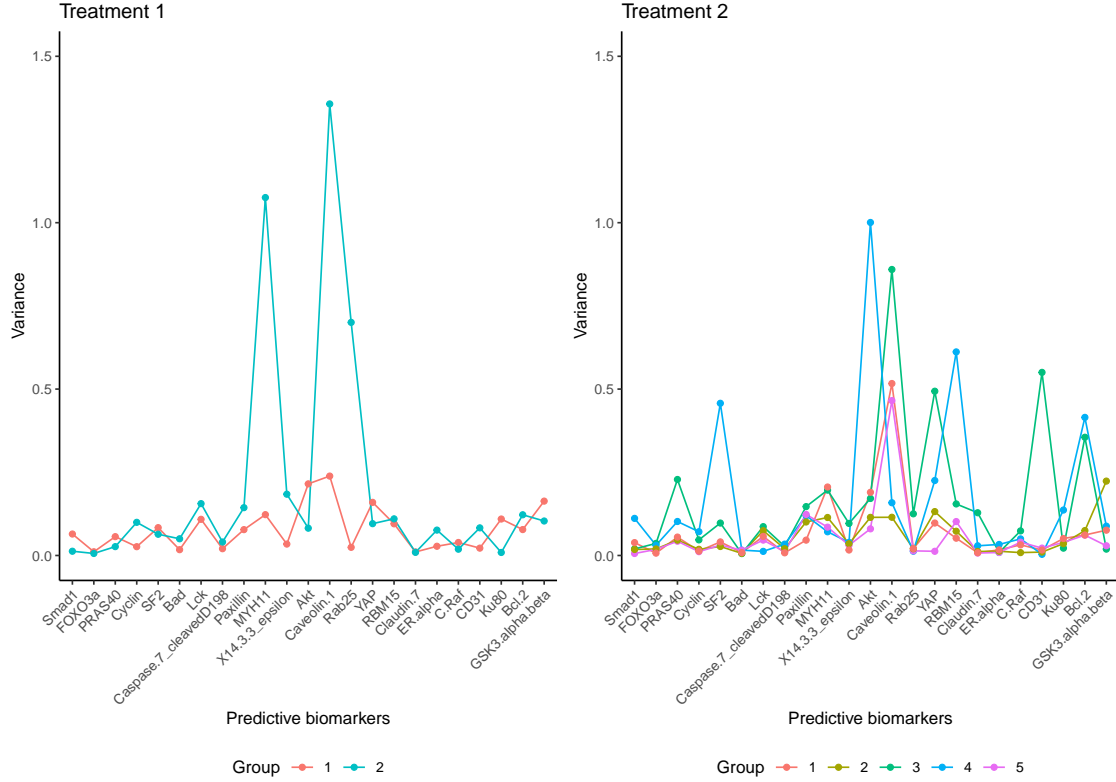


Figure 7: Group-specific variance of predictive biomarkers for patients that received Treatment 1 (left) and Treatment 2 (right). Groups T1G3, T1G5, and T2G9 are singleton and are not displayed.

References

- Agresti, A. (2019). *An introduction to categorical data analysis*. John Wiley & Sons. [3](#)
- Argiento, R., Bianchini, I., and Guglielmi, A. (2016). A blocked gibbs sampler for ngg-mixture models via a priori truncation. *Statistics and Computing*, 26(3):641–661. [5](#), [16](#)
- Argiento, R., Corradin, R., Guglielmi, A., and Lanzarone, E. (2022). Clustering blood donors via mixtures of product partition models with covariates. *arXiv*. [2](#), [5](#), [18](#)
- Argiento, R. and De Iorio, M. (2022). Is infinity that far? a bayesian nonparametric perspective of finite mixture models. *The Annals of Statistics*, 50(5):2641–2663. [19](#)
- Barcella, W., De Iorio, M., and Baio, G. (2017). A comparative review of variable selection techniques for covariate dependent dirichlet process mixture models. *Canadian Journal of Statistics*, 45(3):254–273. [11](#)
- Bedard, P. L., Hansen, A. R., Ratain, M. J., and Siu, L. L. (2013). Tumour heterogeneity in the clinic. *Nature*, 501(7467):355–364. [1](#)
- Bonetti, M. and Gelber, R. D. (2000). A graphical method to assess treatment–covariate interactions using the cox model on subsets of the data. *Statistics in Medicine*, 19(19):2595–2609. [1](#)
- Carvalho, C. M., Polson, N. G., and Scott, J. G. (2010). The horseshoe estimator for sparse signals. *Biometrika*, 97(2):465–480. [3](#)
- Chen, J. and Li, H. (2013). Variable selection for sparse dirichlet-multinomial regression with an application to microbiome data analysis. *The Annals of Applied Statistics*, 7(1):418–442. [3](#)
- Christensen, R., Johnson, W., Branscum, A., and Hanson, T. E. (2011). *Bayesian ideas and data analysis: an introduction for scientists and statisticians*. CRC press. [13](#)
- Claus, E. B., Walsh, K. M., Wiencke, J. K., Molinaro, A. M., Wiemels, J. L., Schildkraut, J. M., Bondy, M. L., Berger, M., Jenkins, R., and Wrensch, M. (2015). Survival and low-grade glioma: the emergence of genetic information. *Neurosurgical Focus*, 38(1):E6. [8](#)

- Corsini, N. and Viroli, C. (2022). Dealing with overdispersion in multivariate count data. *Computational Statistics & Data Analysis*, 170:107447. 3
- De Blasi, P., Favaro, S., Lijoi, A., Mena, R. H., Prünster, I., and Ruggiero, M. (2013). Are gibbs-type priors the most natural generalization of the dirichlet process? *IEEE Transactions on Pattern Analysis and Machine Intelligence*, 37(2):212–229. 4, 16
- Favaro, S., Teh, Y. W., et al. (2013). Mcmc for normalized random measure mixture models. *Statistical Science*, 28(3):335–359. 5, 16, 19, 20, 21
- Gelman, A. and Rubin, D. B. (1992). Inference from iterative simulation using multiple sequences. *Statistical Science*, pages 457–472. 26
- Gnedin, A. and Pitman, J. (2006). Exchangeable gibbs partitions and stirling triangles. *Journal of Mathematical Sciences*, 138(3):5674–5685. 4
- Golub, T. R., Slonim, D. K., Tamayo, P., Huard, C., Gaasenbeek, M., Mesirov, J. P., Coller, H., Loh, M. L., Downing, J. R., Caligiuri, M. A., et al. (1999). Molecular classification of cancer: class discovery and class prediction by gene expression monitoring. *Science*, 286(5439):531–537. 17, 23, 24
- Goodenberger, M. L. and Jenkins, R. B. (2012). Genetics of adult glioma. *Cancer Genetics*, 205(12):613–621. 8
- Hartigan, J. A. (1990). Partition models. *Communications in Statistics-Theory and Methods*, 19(8):2745–2756. 4
- Imai, K., King, G., and Stuart, E. A. (2008). Misunderstandings between experimentalists and observationalists about causal inference. *Journal of the royal statistical society: series A (statistics in society)*, 171(2):481–502. 26
- Ius, T., Ciani, Y., Ruaro, M. E., Isola, M., Sorrentino, M., Bulfoni, M., Candotti, V., Correcig, C., Bourkoula, E., Manini, I., et al. (2018). An nf- κ b signature predicts low-grade glioma prognosis: A precision medicine approach based on patient-derived stem cells. *Neuro-oncology*, 20(6):776–787. 8
- Kosorok, M. R. and Laber, E. B. (2019). Precision medicine. *Annual Review of Statistics and its Application*, 6:263–286. 1
- Lee, J., Thall, P. F., Lim, B., and Msaouel, P. (2022). Utility-based bayesian personalized treatment selection for advanced breast cancer. *Journal of the Royal Statistical Society: Series C (Applied Statistics)*. 6
- Li, S.-Z., Hu, Y.-Y., Zhao, J.-L., Zang, J., Fei, Z., Han, H., and Qin, H.-Y. (2020). Downregulation of fh11 protein in glioma inhibits tumor growth through pi3k/akt signaling. *Oncology Letters*, 19(6):3781–3788. 10
- Lijoi, A., Mena, R. H., and Prünster, I. (2007). Controlling the reinforcement in bayesian non-parametric mixture models. *Journal of the Royal Statistical Society: Series B (Statistical Methodology)*, 69(4):715–740. 2, 4, 5, 16
- Ma, J., Hobbs, B. P., and Stingo, F. C. (2015). Statistical methods for establishing personalized treatment rules in oncology. *BioMed Research International*, 2015. 1
- Ma, J., Hobbs, B. P., and Stingo, F. C. (2018). Integrating genomic signatures for treatment selection with bayesian predictive failure time models. *Statistical Methods in Medical Research*, 27(7):2093–2113. 2
- Ma, J., Stingo, F. C., and Hobbs, B. P. (2016). Bayesian predictive modeling for genomic based personalized treatment selection. *Biometrics*, 72(2):575–583. 2, 3, 6, 8, 14, 23, 24, 25
- Ma, J., Stingo, F. C., and Hobbs, B. P. (2019). Bayesian personalized treatment selection strategies that integrate predictive with prognostic determinants. *Biometrical Journal*, 61(4):902–917. 2, 6, 8, 11, 14, 23, 24, 25, 26, 27
- Mills, C. N., Nowsheen, S., Bonner, J. A., and Yang, E. S. (2011). Emerging roles of glycogen synthase kinase 3 in the treatment of brain tumors. *Frontiers in Molecular Neuroscience*, 4:47. 10
- Monti, S., Tamayo, P., Mesirov, J., and Golub, T. (2003). Consensus clustering: a resampling-based method for class discovery and visualization of gene expression microarray data. *Machine learning*, 52(1):91–118. 6
- Müller, P., Quintana, F., and Rosner, G. L. (2011). A product partition model with regression on covariates. *Journal of Computational and Graphical Statistics*, 20(1):260–278. 2, 4, 5, 23
- Neal, R. M. (2000). Markov chain sampling methods for dirichlet process mixture models. *Journal of Computational and Graphical Statistics*, 9(2):249–265. 5, 19, 20, 21
- Neal, R. M. (2003). Slice sampling. *The Annals of Statistics*, 31(3):705–767. 19, 23
- Olar, A. and Sulman, E. P. (2015). Molecular markers in low-grade glioma—toward tumor reclassification. In *Seminars in Radiation Oncology*, volume 25, pages 155–163. Elsevier. 8
- Page, G. L. and Quintana, F. A. (2015). Predictions based on the clustering of heterogeneous functions via shape and subject-specific covariates. *Bayesian Analysis*, 10(2):379–410. 21

- Page, G. L. and Quintana, F. A. (2016). Spatial product partition models. *Bayesian Analysis*, 11(1):265–298. 5, 23
- Page, G. L. and Quintana, F. A. (2018). Calibrating covariate informed product partition models. *Statistics and Computing*, 28(5):1009–1031. 5, 15, 18
- Page, G. L., Quintana, F. A., and Rosner, G. L. (2021). Discovering interactions using covariate informed random partition models. *The Annals of Applied Statistics*, 15(1):1 – 21. 28
- Pocock, S. J., Assmann, S. E., Enos, L. E., and Kasten, L. E. (2002). Subgroup analysis, covariate adjustment and baseline comparisons in clinical trial reporting: current practice and problems. *Statistics in Medicine*, 21(19):2917–2930. 2
- Polson, N. G., Scott, J. G., and Windle, J. (2014). The bayesian bridge. *Journal of the Royal Statistical Society: Series B (Statistical Methodology)*, 76(4):713–733. 19, 22
- Poux-Médard, G., Velcin, J., and Loudcher, S. (2021). Powered dirichlet process for controlling the importance of “rich-get-richer” prior assumptions in bayesian clustering. *arXiv preprint arXiv:2104.12485*. 16
- Quintana, F. A. and Iglesias, P. L. (2003). Bayesian clustering and product partition models. *Journal of the Royal Statistical Society: Series B (Statistical Methodology)*, 65(2):557–574. 4
- Ripley, B., Venables, B., Bates, D. M., Hornik, K., Gebhardt, A., Firth, D., and Ripley, M. B. (2013). Package ‘mass’. *Cran r*, 538:113–120. 26
- Simon, R. (2010). Clinical trial designs for evaluating the medical utility of prognostic and predictive biomarkers in oncology. *Personalized Medicine*, 7(1):33–47. 1
- Song, X. and Pepe, M. S. (2004). Evaluating markers for selecting a patient’s treatment. *Biometrics*, 60(4):874–883. 1, 8, 25
- Stuart, E. A., King, G., Imai, K., and Ho, D. (2011). Matchit: nonparametric preprocessing for parametric causal inference. *Journal of statistical software*. 26
- Wade, S. and Ghahramani, Z. (2018). Bayesian cluster analysis: Point estimation and credible balls (with discussion). *Bayesian Analysis*, 13(2):559–626. 9, 13, 23
- Zhang, B., Tsiatis, A. A., Laber, E. B., and Davidian, M. (2012). A robust method for estimating optimal treatment regimes. *Biometrics*, 68(4):1010–1018. 2
- Zhao, Y., Zeng, D., Rush, A. J., and Kosorok, M. R. (2012). Estimating individualized treatment rules using outcome weighted learning. *Journal of the American Statistical Association*, 107(499):1106–1118. 2